

# Primitive Pythagorean triples and neutrino mixing

Yuta Hyodo\*

*Graduate School of Science and Technology, Tokai University,  
4-1-1 Kitakaname, Hiratsuka, Kanagawa 259-1292, Japan and  
Micro/Nano Technology Center, Tokai University,  
4-1-1 Kitakaname, Hiratsuka, Kanagawa 259-1292, Japan*

Teruyuki Kitabayashi†

*Department of Physics, Tokai University,  
4-1-1 Kitakaname, Hiratsuka,  
Kanagawa 259-1292, Japan  
(Dated: May 31, 2024)*

The primitive Pythagorean triples are the three natural numbers  $(a, b, c)$  that satisfy  $c^2 = a^2 + b^2$  in a right triangle. We constructed a neutrino mixing models related to primitive Pythagorean triples that satisfy the observed values within the  $3\sigma$  region for the reactor, solar, and atmospheric neutrino mixing angles, as well as the Dirac CP phase.

PACS numbers:

Keywords:

## I. INTRODUCTION

The primitive Pythagorean triples[1–9] are the three natural numbers  $(a, b, c)$  that satisfy  $c^2 = a^2 + b^2$  in the right triangle (Fig. 1). The most famous primitive Pythagorean triple is the combination  $(3, 4, 5)$ . The internal angles of a triangle with the combination  $(3, 4, 5)$  are  $(36.87^\circ, 53.13^\circ, 90.00^\circ)$ . The two internal angles

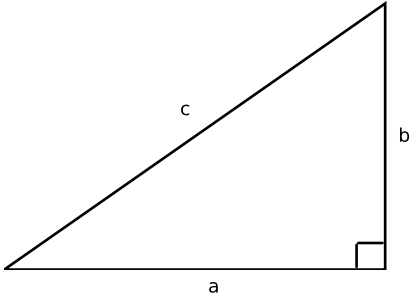


FIG. 1: Right triangle.

$(36.87^\circ, 53.13^\circ)$  closely approximate the upper limit of

\*Corresponding author: 2CTAD004@mail.u-tokai.ac.jp

†Electronic address: teruyuki@tokai-u.jp

the  $3\sigma$  region for the so-called solar neutrino mixing angle,  $35.74^\circ$ , and the upper limit of the  $3\sigma$  region for the so-called atmospheric neutrino mixing angle,  $51.0^\circ$  ( $51.5^\circ$ ), in the case of normal mass ordering (NO) [inverted mass ordering (IO)]. In this paper, we constructed a neutrino mixing model for the solar and atmospheric mixing angles with primitive Pythagorean triples.

The rest of the paper is organized as follows. In Section. II, we review the Pontecorvo-Maki-Nakagawa-Sakata (PMNS) mixing matrix and observed values to compare the mixing model with observed values. In Section. III describes the construction of a neutrino mixing model related to primitive Pythagorean triples. In Section. IV presents the numerical calculation results of the neutrino mixing model constructed in Section. III. In Section. V describes the investigation of if the neutrino mass matrix from the proposed neutrino mixing model is invariant under  $Z_2$  symmetry. Section. VI presents the summary.

## II. PMNS MATRIX

We review the PMNS mixing matrix[10–13] and observed values.

PMNS matrix is written as

$$U = \begin{pmatrix} U_{e1} & U_{e2} & U_{e3} \\ U_{\mu1} & U_{\mu2} & U_{\mu3} \\ U_{\tau1} & U_{\tau2} & U_{\tau3} \end{pmatrix}$$

$$= \begin{pmatrix} c_{12}c_{13} & s_{12}c_{13} & s_{13}e^{-i\delta} \\ -s_{12}c_{23} - c_{12}s_{23}s_{13}e^{i\delta} & c_{12}c_{23} - s_{12}s_{23}s_{13}e^{i\delta} & s_{23}c_{13} \\ s_{12}s_{23} - c_{12}c_{23}s_{13}e^{i\delta} & -c_{12}s_{23} - s_{12}c_{23}s_{13}e^{i\delta} & c_{23}c_{13} \end{pmatrix}, \quad (1)$$

where,  $c_{ij} = \cos \theta_{ij}$ ,  $s_{ij} = \sin \theta_{ij}$  ( $i, j=1,2,3$ ),  $\theta_{ij}$  is a mixing angle, and  $\delta$  is the Dirac CP phase. The sines and cosines of the three neutrino mixing angles of the PMNS matrix,  $U$ , are given by

$$\begin{aligned} s_{12}^2 &= \frac{|U_{e2}|^2}{1 - |U_{e3}|^2}, \quad s_{23}^2 = \frac{|U_{\mu 3}|^2}{1 - |U_{e3}|^2}, \quad s_{13}^2 = |U_{e3}|^2, \\ c_{12}^2 &= \frac{|U_{e1}|^2}{1 - |U_{e3}|^2}, \quad c_{23}^2 = \frac{|U_{\tau 3}|^2}{1 - |U_{e3}|^2}. \end{aligned} \quad (2)$$

The Jarlskog rephasing invariant[14],

$$J = \text{Im}(U_{e1}U_{e2}^*U_{\mu 1}^*U_{\mu 2}) = s_{12}s_{23}s_{13}c_{12}c_{23}c_{13}^2 \sin \delta \quad (3)$$

can be used to calculate  $\delta$ .

A global analysis of current data reveals the following the best-fit values of the neutrino mixing angles in the case of NO,  $m_1 < m_2 < m_3$ , where  $m_1, m_2$ , and  $m_3$  are the neutrino mass eigenvalues, [15]:

$$\begin{aligned} s_{12}^2 &= 0.303_{-0.012}^{+0.012} \quad (0.270 \sim 0.341), \\ s_{23}^2 &= 0.451_{-0.016}^{+0.019} \quad (0.408 \sim 0.603), \\ s_{13}^2 &= 0.02225_{-0.00059}^{+0.00056} \quad (0.02052 \sim 0.02398), \\ \delta/^\circ &= 232_{-26}^{+36} \quad (144 \sim 350), \end{aligned} \quad (4)$$

where the  $\pm$  denotes the  $1\sigma$  region and the parentheses denote the  $3\sigma$  region. For the IO,  $m_3 < m_1 < m_2$ , we have

$$\begin{aligned} s_{12}^2 &= 0.303_{-0.012}^{+0.012} \quad (0.270 \sim 0.341), \\ s_{23}^2 &= 0.569_{-0.021}^{+0.016} \quad (0.412 \sim 0.613), \\ s_{13}^2 &= 0.02223_{-0.00058}^{+0.00058} \quad (0.02048 \sim 0.02416), \\ \delta/^\circ &= 276_{-29}^{+22} \quad (194 \sim 344). \end{aligned} \quad (5)$$

### III. PRIMITIVE PRIMITIVE PYTHAGOREAN TRIPLES AND NEUTRINO MIXING MODEL

#### A. Primitive primitive Pythagorean triples

Primitive Pythagorean triples are the combinations  $(a, b, c)$  of three natural numbers that satisfy  $a^2 + b^2 = c^2$ . The relationship among  $a, b, c$  is described by

$$a < b < c. \quad (6)$$

$a, b, c$  can be expressed in terms of two natural numbers,  $m$  and  $n$ , using either

$$(a, b, c) = (m^2 - n^2, 2mn, m^2 + n^2) \quad (7)$$

or

$$(a, b, c) = (2mn, m^2 - n^2, m^2 + n^2) \quad (8)$$

[2–4]. In the case of Eq. (7) (Eq. (8)),  $a$  is an odd (even) number, and  $b$  is an even (odd) number.

The relationship between  $m$  and  $n$  is as follows[2–4]:

- $m > n$
- $m$  and  $n$  are natural numbers.
- The parities of  $m$  and  $n$ . (one is an odd number; and the other is an even number)
- $m$  and  $n$  are coprime.

#### B. Relationship between the solar mixing angle, atmospheric mixing angle, and primitive Pythagorean triples

The mixing matrix predicting a reactor mixing angle ( $\theta_{13}$ ) of 0 can be written as

$$U = R_{23}R_{12}. \quad (9)$$

$R_{23}$  ( $R_{12}$ ) is a rotation matrix for the 2-3 (1-2) plane[13]; it is denoted by

$$R_{23} = \begin{pmatrix} 1 & 0 & 0 \\ 0 & \cos \theta_{23} & \sin \theta_{23} \\ 0 & -\sin \theta_{23} & \cos \theta_{23} \end{pmatrix}, \quad (10)$$

$$R_{12} = \begin{pmatrix} \cos \theta_{12} & \sin \theta_{12} & 0 \\ -\sin \theta_{12} & \cos \theta_{12} & 0 \\ 0 & 0 & 1 \end{pmatrix}. \quad (11)$$

The relationship between primitive Pythagorean triples and neutrino mixing angles,  $\theta_{12}$  and  $\theta_{23}$ , is as follows:

$$s_{12} = \frac{a}{c}, \quad s_{23} = \frac{b}{c}. \quad (12)$$

With the relationship provided in Eq. (12), the mixing matrix predicting a reactor mixing angle of 0 can be written as

$$U_{\text{PM}} = \begin{pmatrix} \frac{b}{c} & \frac{a}{c} & 0 \\ -\frac{a^2}{c^2} & \frac{ab}{c^2} & \frac{b}{c} \\ -\frac{ab}{c^2} & -\frac{b^2}{c^2} & \frac{a}{c} \end{pmatrix}. \quad (13)$$

We call this mixing matrix primitive Pythagorean triple neutrino mixing (PM).

The mixing matrix predicts the vanishing reactor mixing angle. Next, we performed modifications to improve the prediction of the reactor mixing angle.

### C. Improved reproducibility of reactor mixing angle

To improve the reproducibility of the reactor mixing angle, we employed the method of changing from tri-bimaximal (TBM) mixing to trimaximal (TM) mixing[16, 17]. Using this method, the first column (second column) of the  $U_{\text{PM}}$  remains unchanged, whereas the

second and third columns (first and third) are adjusted.

#### 1. Modifications of the second and third columns

As shown in Ref. [16], the first column of the  $U_{\text{PM}}$  remains unchanged, whereas the second and third columns are adjusted as follows:

$$\begin{aligned} (U_{\text{PM}})_{\text{C1}} &= U_{\text{PM}} U_{23} \\ &= \begin{pmatrix} \frac{b}{c} & \frac{a}{c} \cos \theta & \frac{a}{c} \sin \theta e^{-i\phi} \\ -\frac{a^2}{c^2} & \frac{b}{c^2} (a \cos \theta - c \sin \theta e^{i\phi}) & \frac{b}{c^2} (c \cos \theta + a \sin \theta e^{-i\phi}) \\ \frac{ab}{c^2} & -\frac{1}{c^2} (b^2 \cos \theta + ac \sin \theta e^{i\phi}) & \frac{1}{c^2} (ac \cos \theta - b^2 \sin \theta e^{-i\phi}) \end{pmatrix}, \end{aligned} \quad (14)$$

where

$$U_{23} = \begin{pmatrix} 1 & 0 & 0 \\ 0 & \cos \theta & \sin \theta e^{-i\phi} \\ 0 & -\sin \theta e^{i\phi} & \cos \theta \end{pmatrix}, \quad (15)$$

$\theta$  denotes a rotation angle, and  $\phi$  denotes a phase parameter.

From Eq. (2), the neutrino mixing angles of  $(U_{\text{PM}})_{\text{C1}}$  are as follows:

$$\begin{aligned} s_{12}^2 &= \frac{a^2 \cos^2 \theta}{c^2 - a^2 \sin^2 \theta}, \\ s_{23}^2 &= \frac{b^2 c^2 \cos^2 \theta + ab^2 (a \sin^2 \theta + c \sin 2\theta \cos \phi)}{c^4 - a^2 c^2 \sin^2 \theta}, \\ s_{13}^2 &= \frac{a^2}{c^2} \sin^2 \theta. \end{aligned} \quad (16)$$

In term of  $s_{13}^2$ , detailing  $s_{12}^2$  and  $s_{23}^2$  leads to

$$\begin{aligned} s_{12}^2 &= \frac{a^2}{c^2} \times \frac{\cos^2 \theta}{1 - s_{13}^2}, \\ s_{23}^2 &= \frac{b^2}{c^3} \times \frac{a \sin 2\theta \cos \phi + c (\cos^2 2\theta + s_{13}^2)}{1 - s_{13}^2}. \end{aligned} \quad (17)$$

From Eq. (3), the Dirac CP phase,  $\delta$ , is written as follows:

$$\begin{aligned} \tan \delta &= \frac{a(c^2 + b^2 + a^2 \cos 2\theta) \sin \phi}{a\{a^2 + (c^2 + b^2) \cos 2\theta\} \cos \phi + c(a-b)(a+b) \sin 2\theta}, \\ (a &= m^2 - n^2, b = 2mn, c = m^2 + n^2), \end{aligned} \quad (18)$$

and

$$\begin{aligned} \tan \delta &= \frac{a(2c^2 - a^2 + a^2 \cos 2\theta) \sin \phi}{-a\{a^2 + (2c^2 - a^2) \cos 2\theta\} \cos \phi + c(b-a)(b+a) \sin 2\theta}, \\ (a &= 2mn, b = m^2 - n^2, c = m^2 + n^2). \end{aligned} \quad (19)$$

#### 2. Modifications first and third columns

As shown in Ref. [17], the second column of the  $U_{\text{PM}}$  remains unchanged, whereas the first and third columns are adjusted as follows:

$$\begin{aligned} (U_{\text{PM}})_{\text{C2}} &= U_{\text{PM}} U_{13} \\ &= \begin{pmatrix} \frac{b}{c} \cos \theta & \frac{a}{c} & \frac{b}{c} \sin \theta e^{-i\phi} \\ -\frac{1}{c^2} (a^2 \cos \theta + bc \sin \theta e^{i\phi}) & \frac{ab}{c^2} & \frac{1}{c^2} (bc \cos \theta - a^2 \sin \theta e^{-i\phi}) \\ \frac{a}{c^2} (b \cos \theta - c \sin \theta e^{i\phi}) & -\frac{b^2}{c^2} & \frac{1}{c^2} (c \cos \theta + b \sin \theta e^{-i\phi}) \end{pmatrix}, \end{aligned} \quad (20)$$

where

$$U_{13} = \begin{pmatrix} \cos \theta & 0 & \sin \theta e^{-i\phi} \\ 0 & 1 & 0 \\ -\sin \theta e^{i\phi} & 0 & \cos \theta \end{pmatrix}, \quad (21)$$

where  $\theta$  denotes a rotation angle, and  $\phi$  denotes a phase parameter.

From Eq. (2), the neutrino mixing angles of  $(U_{\text{PM}})_{\text{C2}}$

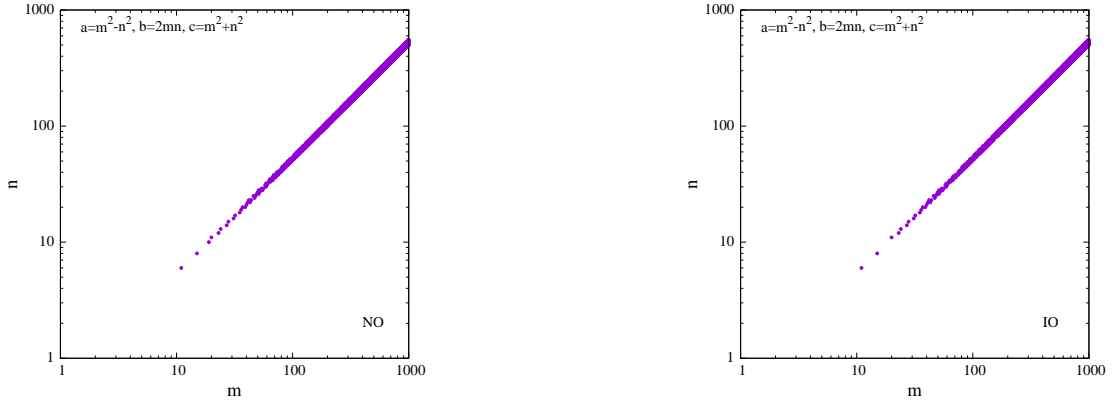


FIG. 2: Dependence of  $m$  on  $n$  of  $(U_{PM})_{C1}$  in the case of  $(a, b, c) = (m^2 - n^2, 2mn, m^2 + n^2)$ .  $\theta$ , and  $\phi$  varied within the ranges of 0 to  $\frac{\pi}{2}$  and 0 to  $2\pi$ , respectively.

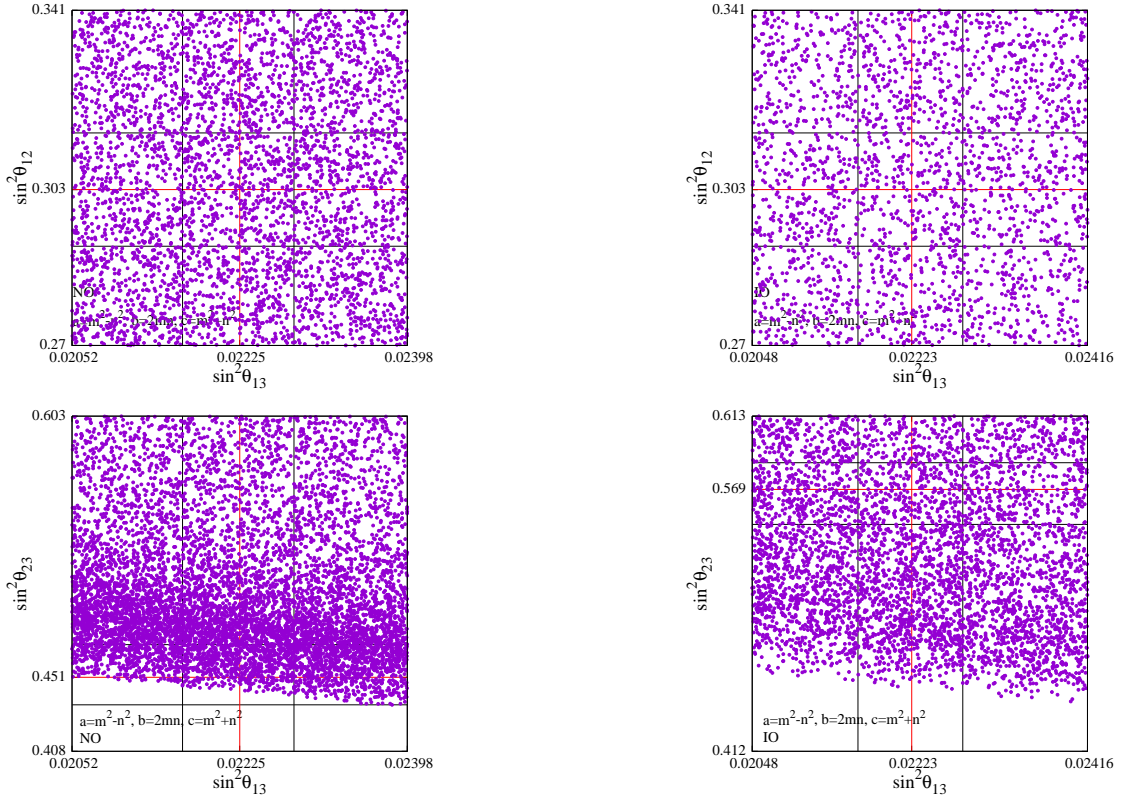


FIG. 3: Dependence of  $s_{12}^2$  and  $s_{23}^2$  on  $s_{13}^2$  of  $(U_{PM})_{C1}$  in the case of  $(a, b, c) = (m^2 - n^2, 2mn, m^2 + n^2)$ .  $\theta$ ,  $\phi$  and  $m$  and  $n$  varied within the ranges of  $0 \sim \frac{\pi}{2}$ , the range of  $\phi$  is varied within  $0 \sim 2\pi$  and the range of  $m$  and  $n$  is varied within 0 to  $\frac{\pi}{2}$  and 0 to  $2\pi$ , and 0  $\sim$  1000, respectively.

are as follows:

$$\begin{aligned} s_{12}^2 &= \frac{a^2}{c^2 - b^2 \sin^2 \theta}, \\ s_{23}^2 &= \frac{b^2 c^2 \cos^2 \theta - a^2 b c \sin 2\theta \cos \phi + a^4 \sin^2 \theta}{c^4 - b^2 c^2 \sin^2 \theta}, \\ s_{13}^2 &= \frac{b^2}{c^2} \sin^2 \theta. \end{aligned} \quad (22)$$

In term of  $s_{13}^2$ , detailing  $s_{12}^2$  and  $s_{23}^2$  leads to

$$\begin{aligned} s_{12}^2 &= \frac{a^2}{c^2} \times \frac{1}{1 - s_{13}^2}, \\ s_{23}^2 &= \frac{b^2 c^2 \cos^2 \theta - a^2 b c \sin 2\theta \cos \phi + a^4 \sin^2 \theta}{c^4 (1 - s_{13}^2)}. \end{aligned} \quad (23)$$

From Eq. (3),  $\delta$  is written as follows:

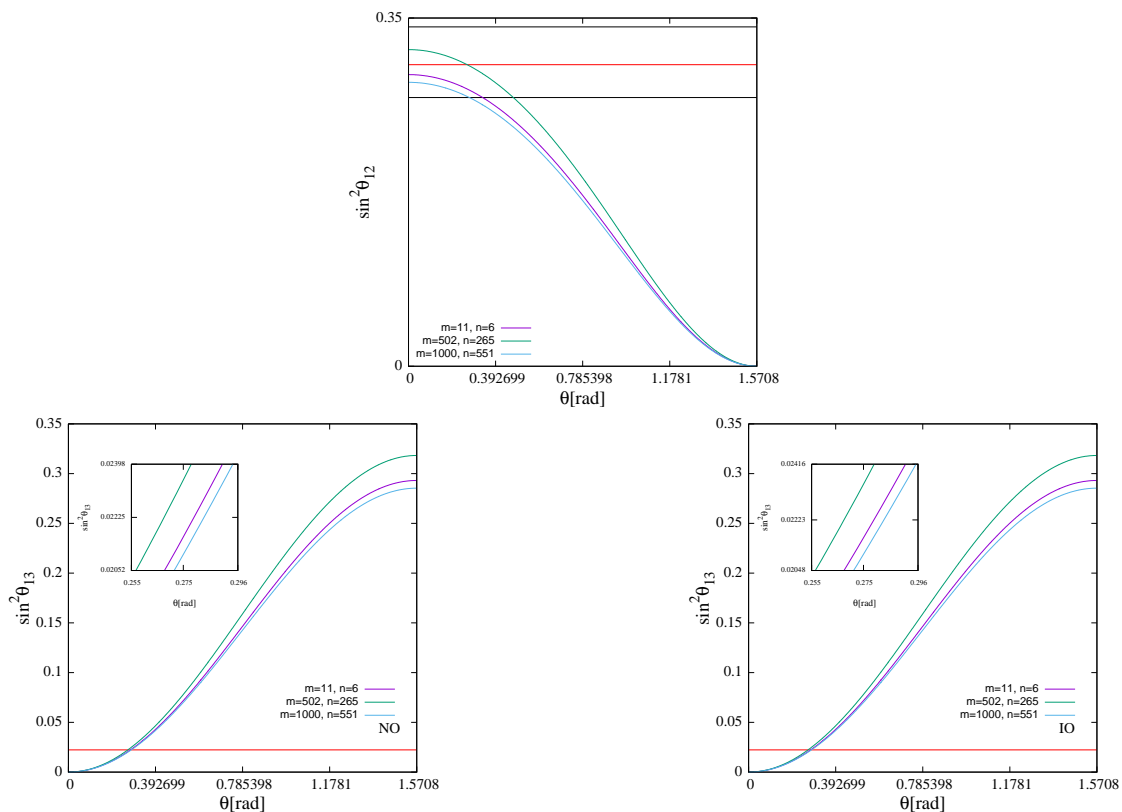


FIG. 4: Dependence of  $s_{12}^2$  and  $s_{13}^2$  on  $\theta$  in the cases of  $m = 11, n = 6$ ,  $m = 502, n = 265$  and  $m = 1000, n = 551$ .

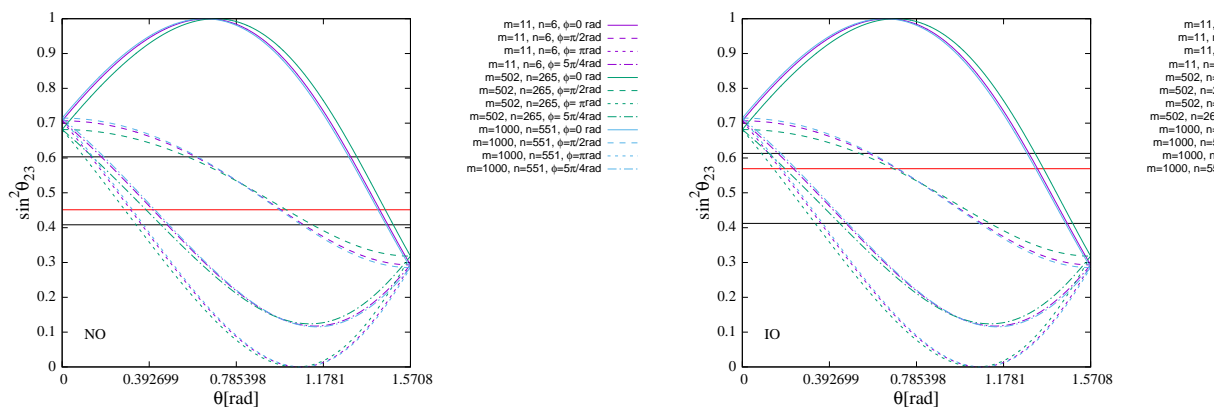


FIG. 5: Dependence of  $s_{23}^2$  on  $\theta$  in the cases of  $m = 11, n = 6$ ,  $m = 502, n = 265$  and  $m = 1000, n = 551$ . We selected  $0, \frac{\pi}{2}, \pi, \frac{5\pi}{4}$  for  $\phi$ .

$$\tan \delta = \frac{b(2c^2 - b^2 + b^2 \cos 2\theta) \sin \phi}{-b\{b^2 + (2c^2 - b^2) \cos 2\theta\} \cos \phi + c(a - b)(a + b) \sin 2\theta},$$

$$(a = m^2 - n^2, b = 2mn, c = m^2 + n^2), \quad (24)$$

and

$$\tan \delta = \frac{b(c^2 + a^2 + b^2 \cos 2\theta) \sin \phi}{b\{b^2 + (c^2 + a^2) \cos 2\theta\} \cos \phi + c(b-a)(b+a) \sin 2\theta},$$

$$(a = 2mn, b = m^2 - n^2, c = m^2 + n^2). \quad (25)$$

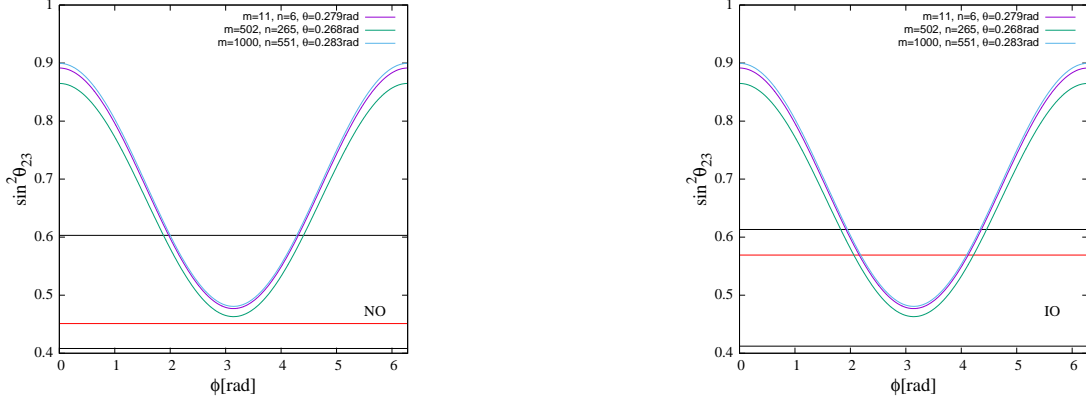


FIG. 6: Dependence of  $s_{23}^2$  on  $\phi$  in the cases of  $m = 11, n = 6$ ,  $m = 502, n = 265$  and  $m = 1000, n = 551$ . We selected  $\theta$  such that  $s_{13}^2$  is approximately 0.022.

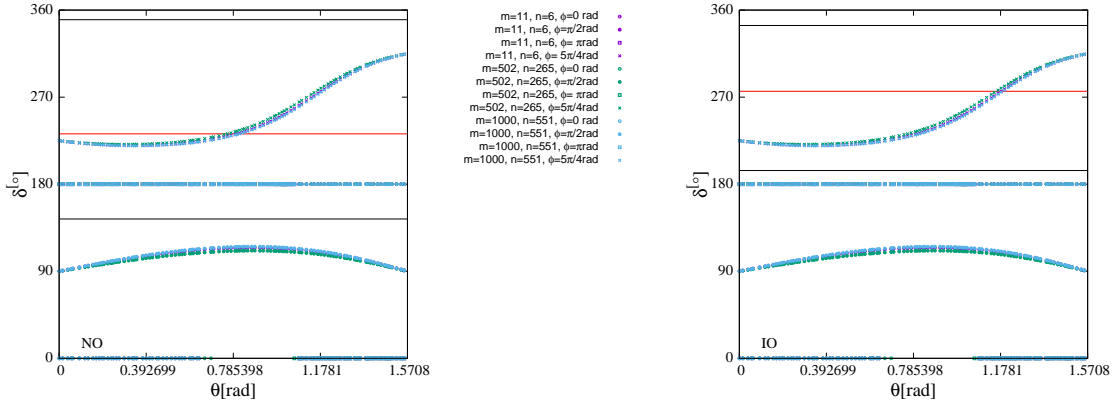


FIG. 7: Dependence of Dirac CP phase  $\delta$  on  $\theta$  in the cases of  $m = 11, n = 6$ ,  $m = 502, n = 265$  and  $m = 1000, n = 551$ . We selected  $0, \frac{\pi}{2}, \pi, \frac{5\pi}{4}$  for  $\phi$ .

Eqs. (18) and (25), as well as Eqs. (19) and (24), are identical. We will algebraically demonstrate this topic in a future study.

#### IV. NUMERICAL CALCULATIONS

First, we performed numerical calculations for  $m$  and  $n$ ,  $\theta$  and  $\phi$  within the ranges of  $1 \sim 1000$ ,  $0$  to  $\frac{\pi}{2}$ , and  $0$  to  $2\pi$ , searching for combinations that satisfy the observed values. Subsequently, we selected three combinations of  $m$  and  $n$  and conducted numerical calculations to investigate the dependence of neutrino parameters on  $\theta$  and  $\phi$ . We investigated the relationship between  $m$  and  $n$  using the Pearson product-moment correlation coefficient

(PPMCC)[18] as follows:

$$r_{mn} = \frac{\sum_{k=1}^l (m_k - \bar{m})(n_k - \bar{n})}{\sqrt{\sum_{k=1}^l (m_k - \bar{m})^2} \sqrt{\sum_{k=1}^l (n_k - \bar{n})^2}}. \quad (26)$$

PPMCC measures the linear correlation between two sets of data within the range of

$$-1 \leq r_{mn} \leq 1. \quad (27)$$

Positive and negative linear correlations are observed as the value approaches 1 and  $-1$ , respectively. If the value is close to 0, no correlation is observed.  $(m_1, n_1), (m_2, n_2), \dots, (m_k, n_k), \dots, (m_l, n_l)$  represents  $l$  sets of data comprising  $m$  and  $n$ , and it becomes  $(m_1, n_1), (m_2, n_2), \dots, (m_k, n_k), \dots, (m_{9716}, n_{9716}) = (11, 6), (15, 8), \dots, (1000, 551)$  (Fig. 2). Furthermore,  $\bar{m}$  and  $\bar{n}$  represent the average, as described in

$$\bar{m} = \frac{\sum_{k=1}^l m_k}{l}, \quad (28)$$

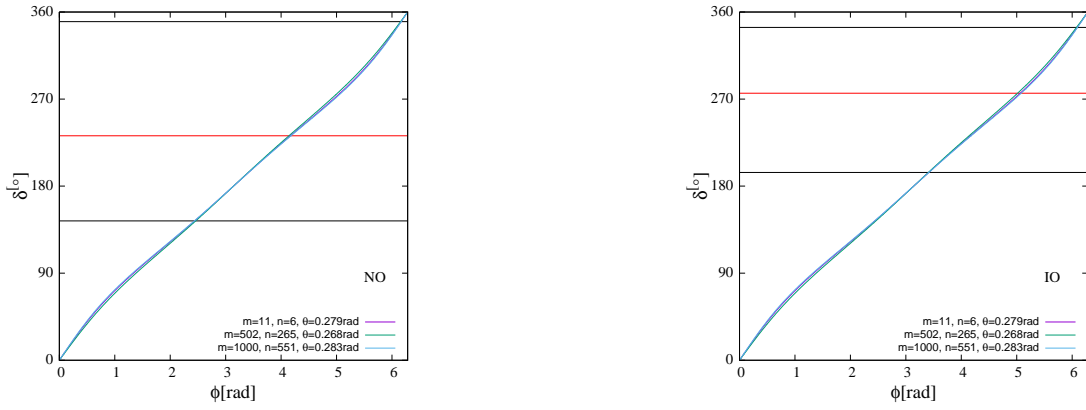


FIG. 8: Dependence of Dirac CP phase  $\delta$  on  $\phi$  in the cases of  $m = 11, n = 6$ ,  $m = 502, n = 265$  and  $m = 1000, n = 551$ . We selected  $\theta$  such that  $s_{13}^2$  is approximately 0.022.

and

$$\bar{n} = \frac{\sum_{k=1}^l n_k}{l}. \quad (29)$$

In the case of Fig. 2,  $l$  is 9716, and the averages of  $m$  and  $n$  are  $\bar{m} = 665$  and  $\bar{n} = 350$ .

If PPMC  $r_{mn}$  is close to 1 (-1), we employed the linear regression model,

$$n = wm + \beta, \quad (30)$$

where  $w$  and  $\beta$  denote the slope and intercept, respectively.

#### A. $(U_{\text{PM}})_{\text{C1}}$

##### 1. The case of the $(a, b, c) = (m^2 - n^2, 2mn, m^2 + n^2)$

Fig. 2 illustrates the dependence of the  $m$  on  $n$  for  $(U_{\text{PM}})_{\text{C1}}$  with the use of  $(a, b, c) = (m^2 - n^2, 2mn, m^2 + n^2)$ . We varied  $\theta$  and  $\phi$  within the ranges of 0 to  $\frac{\pi}{2}$ , and 0 to  $2\pi$ , respectively.

Fig. 2 shows  $m$  and  $n$  satisfying the  $3\sigma$  region for mixing angles,  $s_{ij}^2$ , and the Dirac CP phase,  $\delta$ . The left and right panels show the NO and IO cases, respectively. The key observations from Fig. 2 are as follows:

- In the NO and IO cases, the PPMCs were both 0.997. Considering that both PPMCs were close to 1, a very strong positive linear correlation was observed between  $m$  and  $n$ .
- The relationship between  $m$  and  $n$  exhibits strong linearity. Thus, using Eq. (30), the slope,  $w$ , was 0.527 and 0.526 in the NO and IO cases, respectively. If  $m$  increased by 10,  $n$  increased by 5. The intercept,  $\beta$ , was  $-0.0869$  and  $-0.104$  in the NO and IO cases, respectively. Slope  $w$  and intercept  $\beta$  did not significantly vary between the NO and IO cases.

Fig. 3 illustrates the relationship between  $s_{12}^2$  and  $s_{13}^2$ , in addition to the relationship between  $s_{23}^2$  and  $s_{13}^2$ , for  $(U_{\text{PM}})_{\text{C1}}$  using  $(a, b, c) = (m^2 - n^2, 2mn, m^2 + n^2)$ , satisfying the  $3\sigma$  regions of mixing angles  $s_{ij}^2$  and the Dirac CP phase,  $\delta$ . We varied  $\theta$ ,  $\phi$ , and  $m$  and  $n$  within the ranges of 0 to  $\frac{\pi}{2}$ , 0 to  $2\pi$ , and  $0 \sim 1000$ , respectively.

The upper (lower) panel shows the relationship between  $s_{12}^2$  and  $s_{13}^2$  ( $s_{23}^2$  and  $s_{13}^2$ ). The upper and lower left panels show the NO case, and the upper and lower right panels show the IO case. The red line in the figure represents the best-fit values of  $s_{12}^2$ ,  $s_{13}^2$ , and  $s_{23}^2$ , and the black line shows the  $3\sigma$  region for  $s_{12}^2$ ,  $s_{13}^2$ , and  $s_{23}^2$ .

- In the NO and IO cases, the predicted values of  $s_{12}^2$ ,  $s_{13}^2$ , and  $s_{23}^2$  from the model fell within the  $3\sigma$  region.
- If we appropriately select  $m$ ,  $n$ , and  $\theta$ , the predicted values of  $s_{12}^2$ ,  $s_{13}^2$ , and  $s_{23}^2$  from the model can simultaneously satisfy the best-fit values.

A benchmark point,

$$(m, n, \theta, \phi) = (11, 6, 0.2892 \text{ rad}, 3.364 \text{ rad}) \quad (31)$$

yields

$$(s_{12}^2, s_{13}^2, s_{23}^2, \delta) = (0.2759, 0.02384, 0.4735, 191.6^\circ). \quad (32)$$

Next, using  $(m, n) = (11, 6), (502, 265), (1000, 551)$ , we investigated the relationship between neutrino mixing angles,  $\delta$ , rotation angle  $\theta$ , and phase parameter  $\phi$ .

Fig. 4 illustrates the dependence of the  $s_{12}^2$  and  $s_{13}^2$  on  $\theta$  in the cases of  $m = 11, n = 6$ ,  $m = 502, n = 265$  and  $m = 1000, n = 551$ . The red line represents the best-fit values of  $s_{12}^2$  and  $s_{13}^2$ , and the black line in the upper panel indicates the  $3\sigma$  region for  $s_{12}^2$ . The enlarged view in the lower panel illustrates the dependence of  $s_{13}^2$  on  $\theta$  when expanded into the  $3\sigma$  region of  $s_{13}^2$ . The key observations from Fig. 4 are as follows:

- $\theta$  exists to satisfy the  $3\sigma$  region of  $s_{13}^2$  and  $s_{12}^2$ .

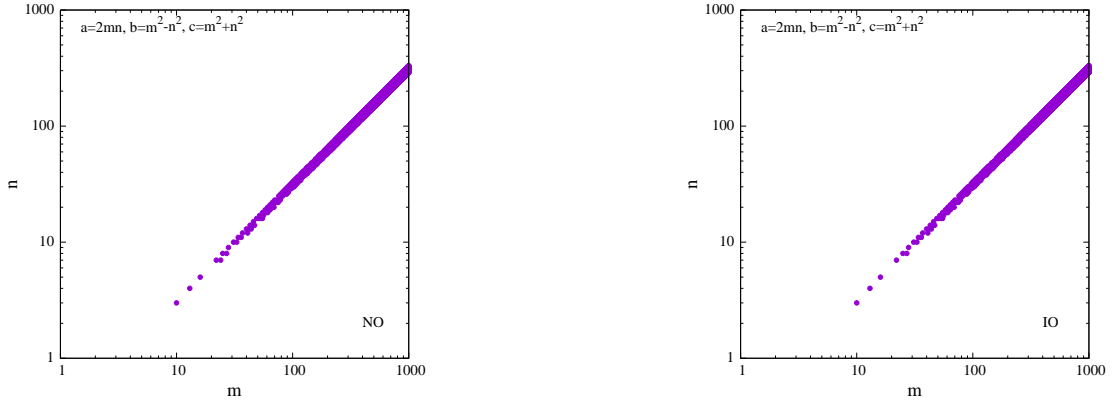


FIG. 9: Similar to Fig. 2, except for  $(a, b, c) = (2mn, m^2 - n^2, m^2 + n^2)$  and  $(U_{\text{PM}})_{C1}$ .

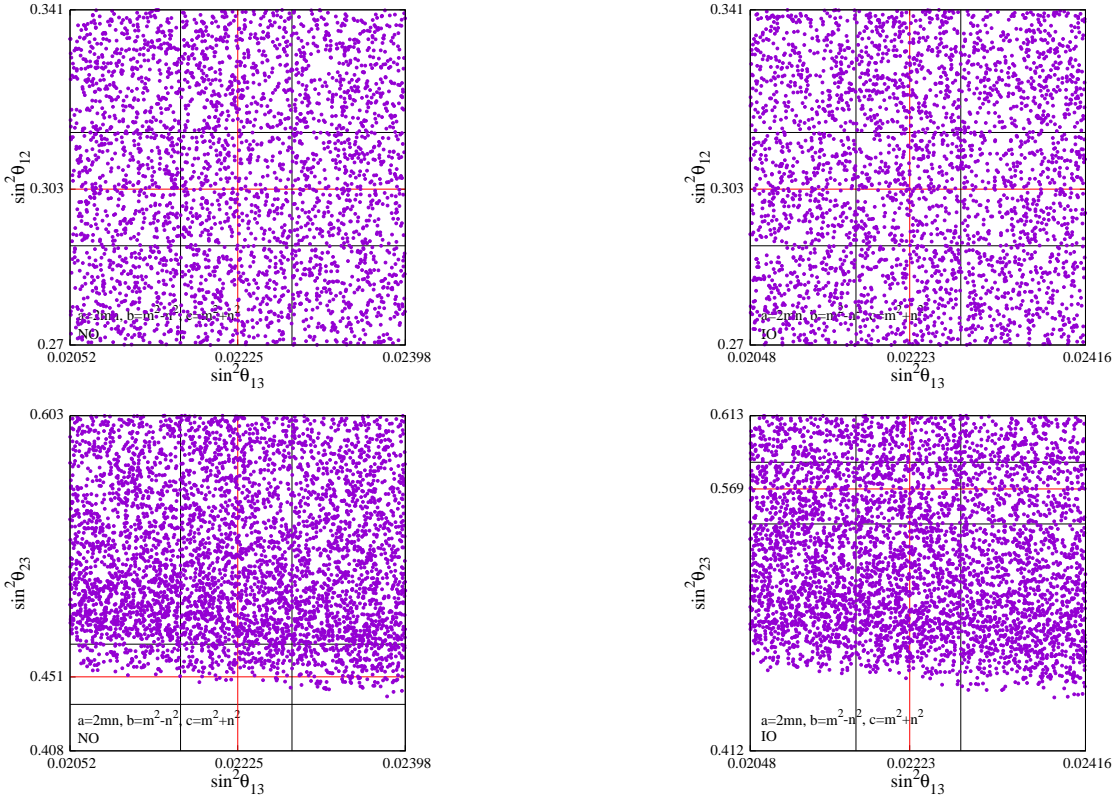


FIG. 10: Similar to Fig. 3, except for  $(a, b, c) = (2mn, m^2 - n^2, m^2 + n^2)$  and  $(U_{\text{PM}})_{C1}$ .

- The range of  $\theta$  satisfying the  $3\sigma$  region of  $s_{13}^2$  was limited to  $0.255 \text{ rad} \leq \theta \leq 0.296 \text{ rad}$ .
- If the range of  $\theta$  was  $0.255 \text{ rad} \leq \theta \leq 0.296 \text{ rad}$ ,  $s_{12}^2$  was within the  $3\sigma$  region of  $s_{12}^2$ .

Fig. 5 illustrates the dependence of  $s_{23}^2$  on  $\theta$  in the cases of  $m = 11, n = 6$ ,  $m = 502, n = 265$  and  $m = 1000, n = 551$ . We selected  $0, \frac{\pi}{2}, \pi, \frac{5\pi}{4}$  for  $\phi$ . The red line represents the best-fit values of  $s_{23}^2$ , and the black line shows the  $3\sigma$  region for  $s_{23}^2$ . The left and right panels show the NO and IO cases, respectively.

Fig. 6 illustrates the dependence of  $s_{23}^2$  on  $\phi$  in the cases of  $m = 11, n = 6$ ,  $m = 502, n = 265$  and  $m = 1000, n = 551$ . We selected  $\theta$  such that  $s_{13}^2$  was approximately 0.022. The left and right panels show the NO and IO cases, respectively. The key observations from Figs.5 and 6 are as follows:

- $\theta$  and  $\phi$  exist to satisfy the  $3\sigma$  region of  $s_{23}^2$ .
- This combination of  $m$  and  $n$  does not satisfy the best-fit value for NO; however, it satisfies the best-fit value for IO.



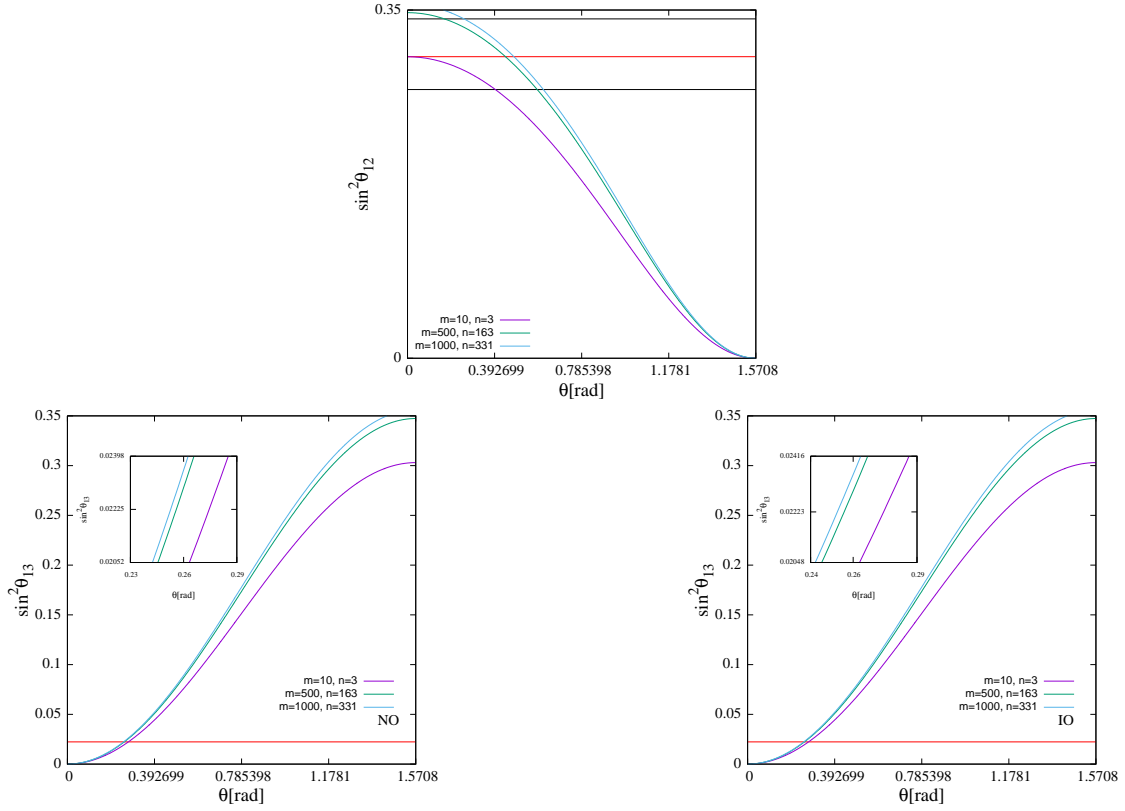


FIG. 11: Similar to Fig. 4, except for  $(a, b, c) = (2mn, m^2 - n^2, m^2 + n^2)$  and  $(U_{PM})_{C1}$ . We selected  $(m, n) = (10, 3), (500, 163), (1000, 331)$ .

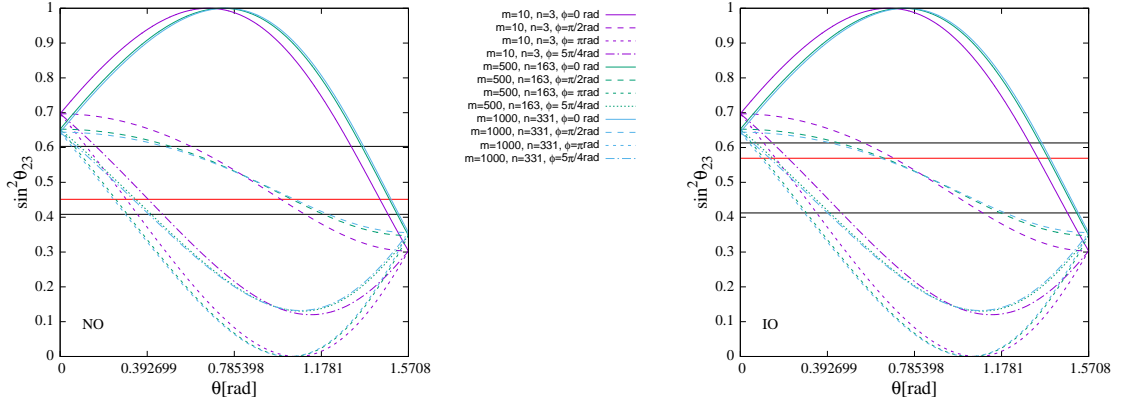


FIG. 12: Similar to Fig. 5, except for  $(a, b, c) = (2mn, m^2 - n^2, m^2 + n^2)$  and  $(U_{PM})_{C1}$ . We selected  $(m, n) = (10, 3), (500, 163), (1000, 331)$ .

- The other  $m$  and  $n$  combinations satisfy the best-fit value of NO. For example, a benchmark point,  $(m, n, \theta, \phi) = (44, 23, 0.2743 \text{ rad}, 3.188 \text{ rad})$ , yields  $(s_{12}^2, s_{13}^2, s_{23}^2, \delta) = (0.3093, 0.02390, 0.4512, 182.5^\circ)$ .

- As shown in Fig. 6, the range of  $\phi$  satisfying the  $3\sigma$  region of  $s_{23}^2$  was limited to  $1.8 \text{ rad} \leq \phi \leq 4.5 \text{ rad}$ .

Fig. 7 illustrates the dependence of  $\delta$  on  $\theta$  in the cases

of  $m = 11, n = 6$ ,  $m = 502, n = 265$  and  $m = 1000, n = 551$ . We selected  $0, \frac{\pi}{2}, \pi, \frac{5\pi}{4}$  for  $\phi$ . The red line represents the best-fit values of  $\delta$ , and the black line shows the  $3\sigma$  region for  $\delta$ . The left and right panels show the IO cases, respectively.

Fig. 8 illustrates the dependence of  $\delta$  on  $\phi$  in the cases of  $m = 11, n = 6$ ,  $m = 502, n = 265$  and  $m = 1000, n = 551$ . We selected  $\theta$  such that  $s_{13}^2$  was approximately 0.022. The left and right panels show the

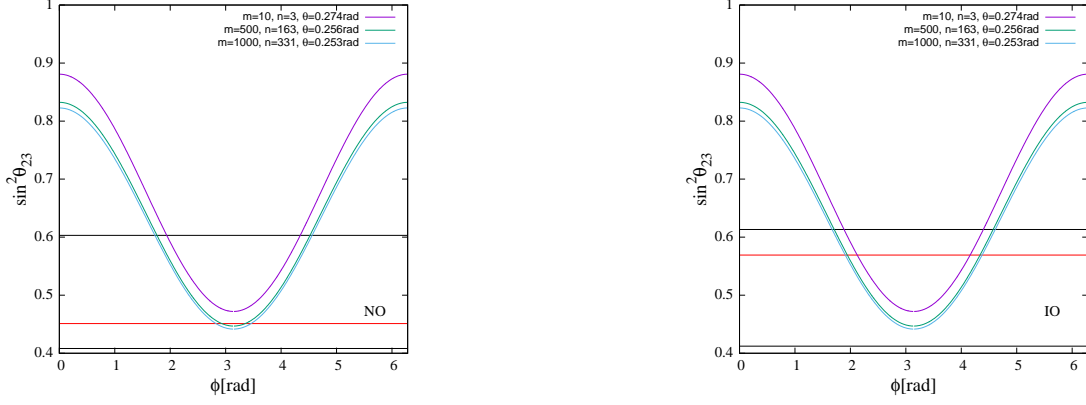


FIG. 13: Similar to Fig. 6, except for  $(a, b, c) = (2mn, m^2 - n^2, m^2 + n^2)$  and  $(U_{PM})_{C1}$ . We selected  $(m, n) = (10, 3), (500, 163), (1000, 331)$ .

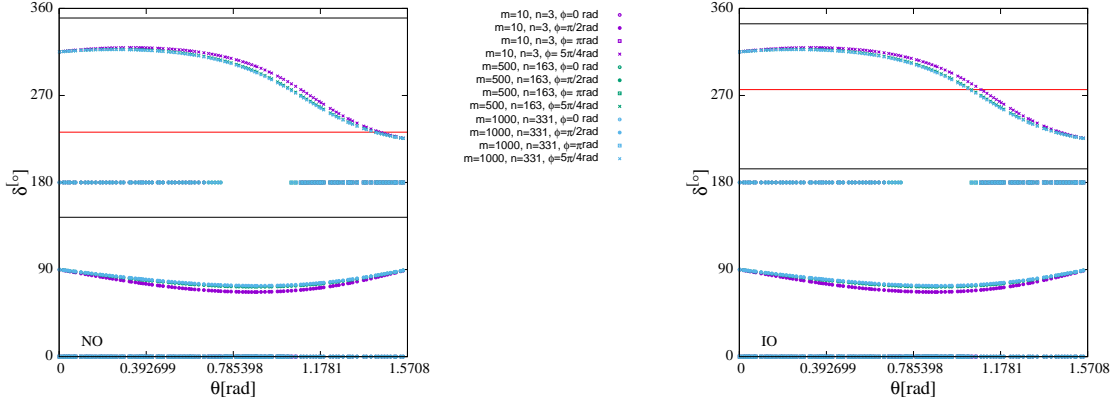


FIG. 14: Similar to Fig. 7, except for  $(a, b, c) = (2mn, m^2 - n^2, m^2 + n^2)$  and  $(U_{PM})_{C1}$ . We selected  $(m, n) = (10, 3), (500, 163), (1000, 331)$ .

NO and IO cases, respectively. The key observations from Figs.7 and 8 are as follows:

- No difference was observed in the  $\delta$  for the different combinations of  $m$  and  $n$ .
- As shown in Fig. 8, the range of  $\phi$  satisfying the  $3\sigma$  region of  $\delta$  was limited to  $2.4 \text{ rad} \leq \phi \leq 6.2 \text{ rad}$ .

## 2. The case of the $(a, b, c) = (2mn, m^2 - n^2, m^2 + n^2)$

Fig. 9 is the same as Fig. 2, except for  $(a, b, c) = (2mn, m^2 - n^2, m^2 + n^2)$  and  $(U_{PM})_{C1}$ . The key observations from Fig. 9 are as follows:

- In the NO and IO cases, the PPMCs were both 0.994. The PPMCs were close to 1; thus, a very strong positive linear correlation was observed between  $m$  and  $n$ .
- The relationship between  $m$  and  $n$  exhibits strong linearity. Thus, using Eq. (30), slope  $w$  was 0.311 in the NO and IO cases, respectively. If  $m$  increased

by 10,  $n$  increased by 3. The intercept  $\beta$  was  $-0.150$  and  $-0.196$  in the NO and IO cases, respectively. Slope  $w$  and intercept  $\beta$  did not significantly vary between the NO and IO cases.

- The slope of Fig. 9 is smaller than that of Fig. 2.

Fig. 10 is the same as Fig. 3, except, for  $(a, b, c) = (2mn, m^2 - n^2, m^2 + n^2)$  and  $(U_{PM})_{C1}$ . The key observations from Fig. 10 are as follows:

- In the NO and IO cases, the predicted values of  $s_{12}^2$ ,  $s_{13}^2$ , and  $s_{23}^2$  from the model fell within the  $3\sigma$  region.
- If we appropriately selected  $m$ ,  $n$  and  $\theta$ , the predicted values of  $s_{12}^2$ ,  $s_{13}^2$ , and  $s_{23}^2$  from the model can simultaneously satisfy the best-fit values.

A benchmark point,

$$(m, n, \theta, \phi) = (10, 3, 0.2785 \text{ rad}, 3.952 \text{ rad}), \quad (33)$$

yields

$$(s_{12}^2, s_{13}^2, s_{23}^2, \delta) = (0.2867, 0.02290, 0.5327, 318.1^\circ). \quad (34)$$

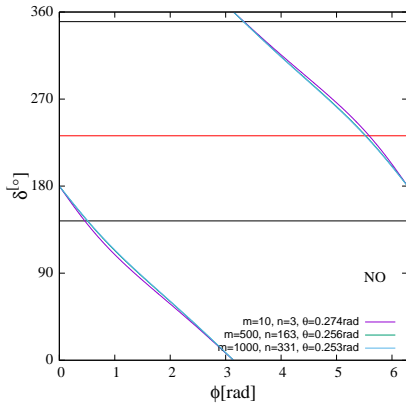


FIG. 15: Similar to Fig. 8, except for  $(a, b, c) = (2mn, m^2 - n^2, m^2 + n^2)$  and  $(U_{\text{PM}})_{C1}$ . We selected  $(m, n) = (10, 3), (500, 163), (1000, 331)$ .

Next, using  $(m, n) = (10, 3), (500, 163), (1000, 331)$ , we investigated the relationship between the neutrino mixing angles,  $\delta$ , rotation angle  $\theta$  and phase parameter  $\phi$ .

Fig. 11 is the same as Fig. 4, except for  $(a, b, c) = (2mn, m^2 - n^2, m^2 + n^2)$  and  $(U_{\text{PM}})_{C1}$ . The key observations from Fig. 11 are as follows:

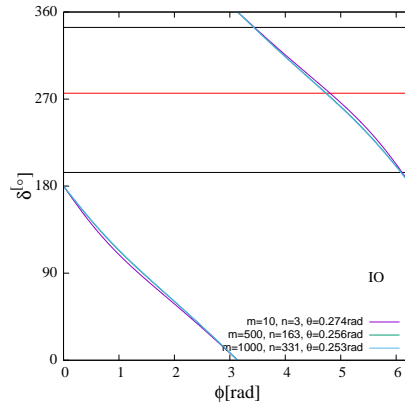
- $\theta$  exists to satisfy the  $3\sigma$  region of  $s_{13}^2$  and  $s_{12}^2$ .
- The range of  $\theta$  satisfying the  $3\sigma$  region of  $s_{13}^2$  was limited to  $0.241 \text{ rad} \leq \theta \leq 0.285 \text{ rad}$ .
- If the range of  $\theta$  is  $0.241 \text{ rad} \leq \theta \leq 0.285 \text{ rad}$ ,  $s_{12}^2$  is within the  $3\sigma$  region of  $s_{12}^2$ .

Fig. 12 is the same as Fig. 5, except for  $(a, b, c) = (2mn, m^2 - n^2, m^2 + n^2)$  and  $(U_{\text{PM}})_{C1}$ . Fig. 13 is the same as Fig. 6, except for  $(a, b, c) = (2mn, m^2 - n^2, m^2 + n^2)$  and  $(U_{\text{PM}})_{C1}$ . The key observations from Figs. 12 and 13 are as follows:

- $\theta$  and  $\phi$  exist to satisfy the  $3\sigma$  region of  $s_{23}^2$ .
- There is a combination of  $m$  and  $n$  that satisfies the best-fit values of NO and IO.
- As shown in Fig. 13, the range of  $\phi$  satisfying the  $3\sigma$  region of  $s_{23}^2$  was limited to  $1.7 \text{ rad} \leq \phi \leq 4.6 \text{ rad}$ .

Fig. 14 is the same as Fig. 7, except for  $(a, b, c) = (2mn, m^2 - n^2, m^2 + n^2)$  and  $(U_{\text{PM}})_{C1}$ . Fig. 15 is the same as Fig. 8, except for  $(a, b, c) = (2mn, m^2 - n^2, m^2 + n^2)$  and  $(U_{\text{PM}})_{C1}$ . The key observations from Fig. 14 and 15 are as follows:

- No difference was observed in the  $\delta$  for different combinations of  $m$  and  $n$ .
- As shown in Fig. 15, the range of  $\phi$  satisfying the  $3\sigma$  region of  $\delta$  was limited to  $0 \text{ rad} \leq \phi \leq 0.5 \text{ rad}$  and  $3.3 \text{ rad} \leq \phi \leq 2\pi \text{ rad}$ .



## B. $(U_{\text{PM}})_{C2}$

### 1. The case of the $(a, b, c) = (m^2 - n^2, 2mn, m^2 + n^2)$

Fig. 16 is the same as Fig. 2, except for  $(a, b, c) = (m^2 - n^2, 2mn, m^2 + n^2)$  and  $(U_{\text{PM}})_{C2}$ . The key observations from Fig. 16 are as follows:

- In the NO and IO cases, the PPMCs were both 0.999. Both PPMCs were close to 1; thus, a very strong positive linear correlation was observed between  $m$  and  $n$ .
- The relationship between  $m$  and  $n$  exhibits strong linearity. Thus, using Eq. (30),  $w$  was 0.527 in both cases. If  $m$  increased by 10,  $n$  increased by 5.  $\beta$  was  $-0.106$  and  $-0.0698$  in the NO and IO cases. Slope  $w$  and intercept  $\beta$  did not significantly vary between the NO and IO cases.

Fig. 17 is the same as Fig. 3, except for  $(a, b, c) = (m^2 - n^2, 2mn, m^2 + n^2)$  and  $(U_{\text{PM}})_{C2}$ . The key observations from Fig. 17 are as follows:

- In the NO and IO cases, the predicted values of  $s_{12}^2$ ,  $s_{13}^2$ , and  $s_{23}^2$  from the model fell within the  $3\sigma$  region.
- The predicted values from the model exceeded or were equal to 0.3 and 0.55 for  $s_{12}^2$  and  $s_{23}^2$ , respectively, in both cases. Thus, it was impossible to simultaneously satisfy the best-fit values for  $s_{12}^2$ ,  $s_{13}^2$  and  $s_{23}^2$  in the case of NO.

A benchmark point,

$$(m, n, \theta, \phi) = (19, 10, 0.1751 \text{ rad}, 0.4214 \text{ rad}) \quad (35)$$

yields

$$(s_{12}^2, s_{13}^2, s_{23}^2, \delta) = (0.3273, 0.02062, 0.5914, 157.1^\circ). \quad (36)$$

Next, using  $(m, n) = (19, 10), (500, 261), (1000, 553)$ , we investigated the relationship between the neutrino

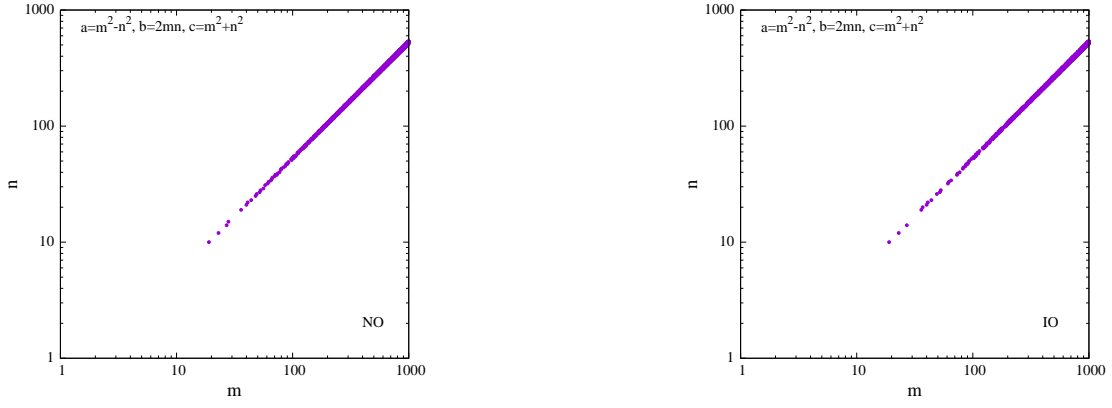


FIG. 16: Similar to Fig. 2, except for  $(a, b, c) = (m^2 - n^2, 2mn, m^2 + n^2)$  and  $(U_{\text{PM}})_{C2}$ .

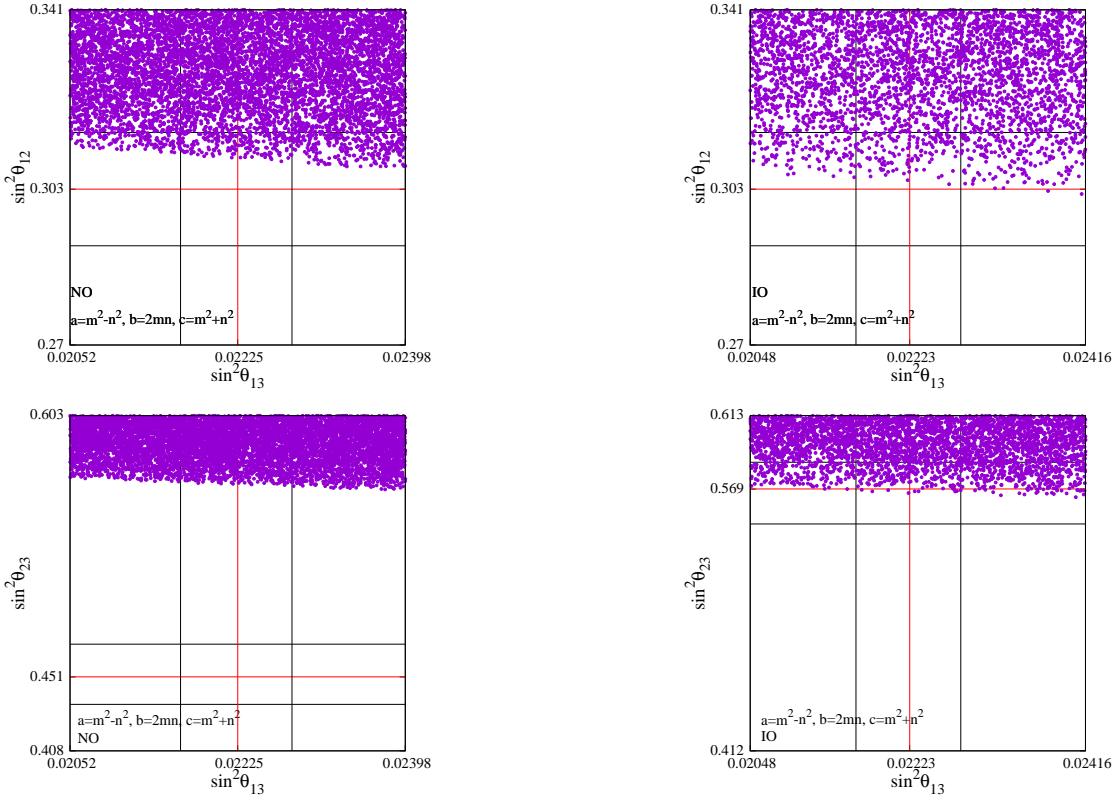


FIG. 17: Similar to Fig. 3, except for  $(a, b, c) = (m^2 - n^2, 2mn, m^2 + n^2)$  and  $(U_{\text{PM}})_{C2}$ .

mixing angles,  $\delta$ , rotation angle  $\theta$ , and phase parameter  $\phi$ .

Fig. 18 is the same as Fig. 4, except for  $(a, b, c) = (2mn, m^2 - n^2, m^2 + n^2)$  and  $(U_{\text{PM}})_{C1}$ . The key observations from Fig. 18 are as follows:

- $\theta$  exists to satisfy the  $3\sigma$  region of  $s_{13}^2$  and  $s_{12}^2$ .
- The range of  $\theta$  satisfying the  $3\sigma$  region of  $s_{13}^2$  was limited to  $0.173 \text{ rad} \leq \theta \leq 0.187 \text{ rad}$ .
- If the range of  $\theta$  was  $0.173 \text{ rad} \leq \theta \leq 0.187 \text{ rad}$ ,

$s_{12}^2$  was within the  $3\sigma$  region of  $s_{12}^2$ . However, it exceeded the best-fit value.

Fig. 19 is the same as Fig. 5, except for  $(a, b, c) = (2mn, m^2 - n^2, m^2 + n^2)$  and  $(U_{\text{PM}})_{C1}$ . Fig. 20 is the same as Fig. 6, except for  $(a, b, c) = (2mn, m^2 - n^2, m^2 + n^2)$  and  $(U_{\text{PM}})_{C1}$ . The key observations from Figs.19 and 20 are as follows:

- $\theta$  and  $\phi$  exist to satisfy the  $3\sigma$  region of  $s_{23}^2$ .
- This combination of  $m$  and  $n$  satisfies the best-fit value for IO.

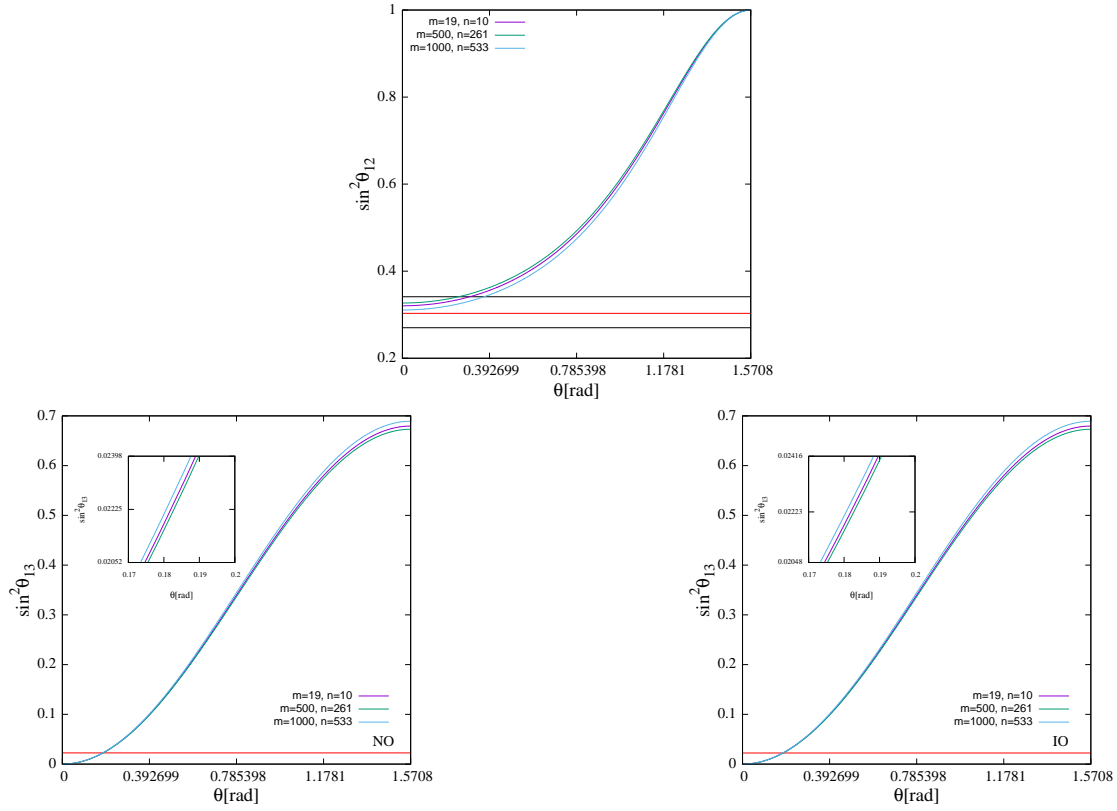


FIG. 18: Similar to Fig. 4, except for  $(a, b, c) = (m^2 - n^2, 2mn, m^2 + n^2)$  and  $(U_{PM})_{C2}$ . We selected  $(m, n) = (19, 10), (500, 261), (1000, 533)$ .

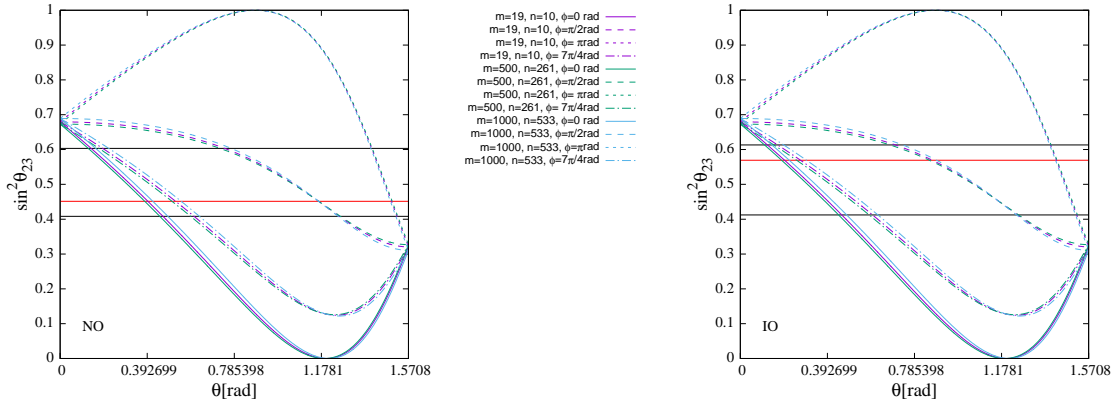


FIG. 19: Similar to Fig. 5, except for  $(a, b, c) = (m^2 - n^2, 2mn, m^2 + n^2)$  and  $(U_{PM})_{C2}$ . We selected  $(m, n) = (19, 10), (500, 261), (1000, 533)$  and  $\phi = 0, \frac{\pi}{2}, \pi, \frac{7\pi}{4}$ .

- This combination of  $m$  and  $n$  does not satisfy the best-fit value for NO.
- If  $s_{13}^2$  aligns with the best-fit value,  $s_{23}^2$  was close to the upper limit of the  $3\sigma$  region.
- As shown in Fig. 20, the range of  $\phi$  satisfying the  $3\sigma$  region of  $s_{23}^2$  was limited to  $0 \text{ rad} \leq \phi \leq 1 \text{ rad}$  and  $5.3 \text{ rad} \leq \phi \leq 2\pi \text{ rad}$ .

Fig. 21 is the same as Fig. 7, except for

$(a, b, c) = (2mn, m^2 - n^2, m^2 + n^2)$  and  $(U_{PM})_{C2}$ . Fig. 22 is the same as Fig. 8, except for  $(a, b, c) = (2mn, m^2 - n^2, m^2 + n^2)$  and  $(U_{PM})_{C2}$ . The key observations from Figs. 21 and 22 are as follows:

- No difference was observed in the  $\delta$  for different combinations of  $m$  and  $n$ .
- As shown in Fig. 22, the range of  $\phi$  satisfying the  $3\sigma$  region of the  $\delta$  was limited to  $0 \text{ rad} \leq \phi \leq$

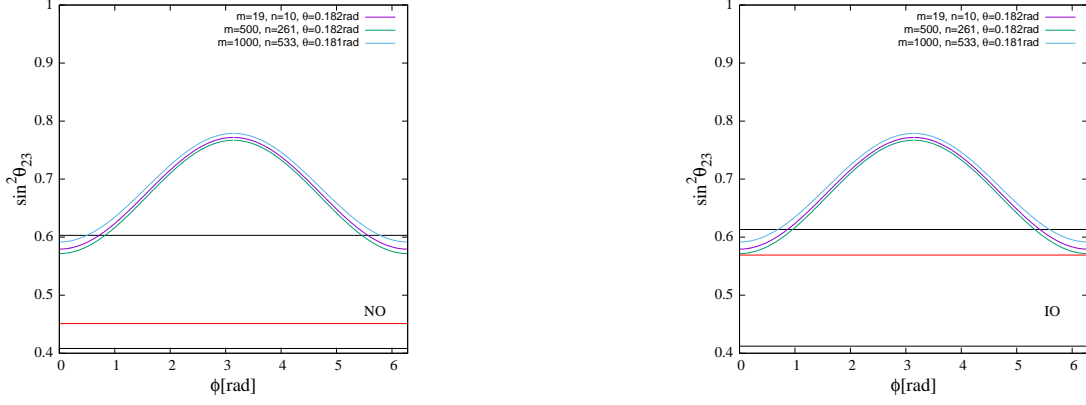


FIG. 20: Similar to Fig. 6, except for  $(a, b, c) = (m^2 - n^2, 2mn, m^2 + n^2)$  and  $(U_{\text{PM}})_{C_2}$ . We selected  $(m, n) = (19, 10), (500, 261), (1000, 553)$ .

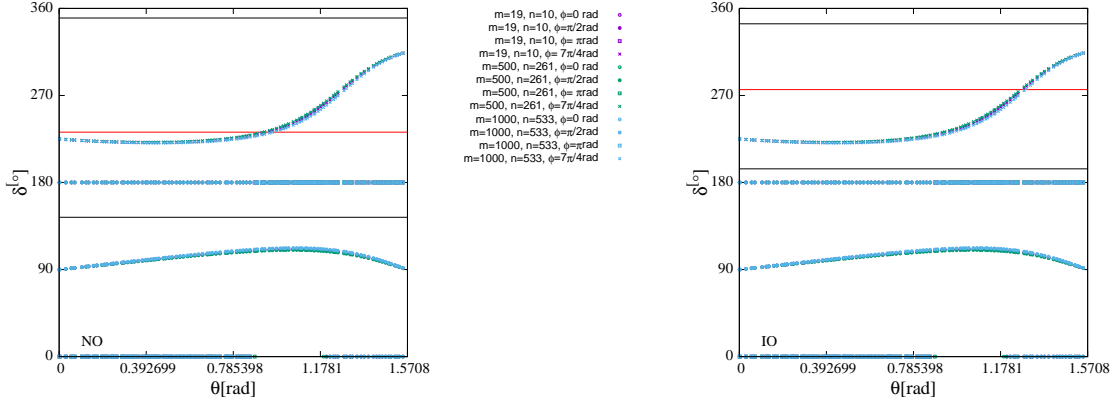


FIG. 21: Similar to Fig. 7, except for  $(a, b, c) = (m^2 - n^2, 2mn, m^2 + n^2)$  and  $(U_{\text{PM}})_{C_2}$ . We selected  $(m, n) = (19, 10), (500, 261), (1000, 553)$  and  $\phi = 0, \frac{\pi}{2}, \pi, \frac{7\pi}{4}$ .

0.6 rad and  $3.3 \text{ rad} \leq \phi \leq 2\pi \text{ rad}$ .

## 2. The case of the $(a, b, c) = (2mn, m^2 - n^2, m^2 + n^2)$

Fig. 23 is the same as Fig. 2, except for  $(a, b, c) = (2mn, m^2 - n^2, m^2 + n^2)$  and  $(U_{\text{PM}})_{C_2}$ . The key observations from Fig. 23 are as follows:

- In the NO and IO cases, the PPMCs were both 0.999. The PPMCs were close to 1; thus, a very strong positive linear correlation was observed between  $m$  and  $n$ .
- The relationship between  $m$  and  $n$  exhibits strong linearity. Thus, using Eq. (30),  $w$  was 0.311 and 0.310 in the NO and IO cases, respectively. If  $m$  increased by 10,  $n$  increased by 3.  $\beta$  was  $-0.0995$  and  $-0.0370$  in the NO and IO cases, respectively.  $w$  and  $\beta$  did not significantly vary between the NO and IO cases.
- The slop of Fig. 23 is smaller than that of Fig. 16.

Fig. 24 is the same as Fig. 3, except for  $(a, b, c) = (m^2 - n^2, 2mn, m^2 + n^2)$  and  $(U_{\text{PM}})_{C_2}$ . The key observations from Fig. 24 are as follows:

- In the NO and IO cases, the predicted values of  $s_{12}^2$ ,  $s_{13}^2$ , and  $s_{23}^2$  from the model fell within the  $3\sigma$  region.
- The predicted values from the model exceeded or were equal to 0.3 for  $s_{12}^2$  and 0.55 for  $s_{23}^2$  in both case. Thus, it was impossible to simultaneously satisfy the best-fit values for  $s_{12}^2$ ,  $s_{13}^2$ , and  $s_{23}^2$  in the case of NO.

A benchmark point,

$$(m, n, \theta, \phi) = (16, 5, 0.1881 \text{ rad}, 5.529 \text{ rad}) \quad (37)$$

yields

$$(s_{12}^2, s_{13}^2, s_{23}^2, \delta) = (0.3321, 0.02363, 0.5986, 319.2^\circ). \quad (38)$$

Next, using  $(m, n) = (16, 5), (500, 153), (1000, 317)$ , we investigated the relationship between the neutrino mixing angles,  $\delta$ , rotation angle  $\theta$ , and phase parameter  $\phi$ .

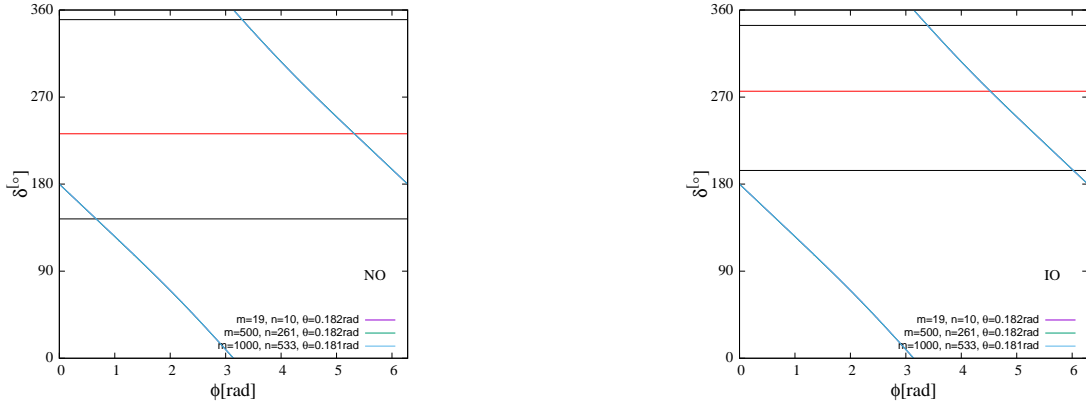


FIG. 22: Similar to Fig. 8, except for  $(a, b, c) = (m^2 - n^2, 2mn, m^2 + n^2)$  and  $(U_{\text{PM}})_{C2}$ . We selected  $(m, n) = (19, 10), (500, 261), (1000, 553)$ .

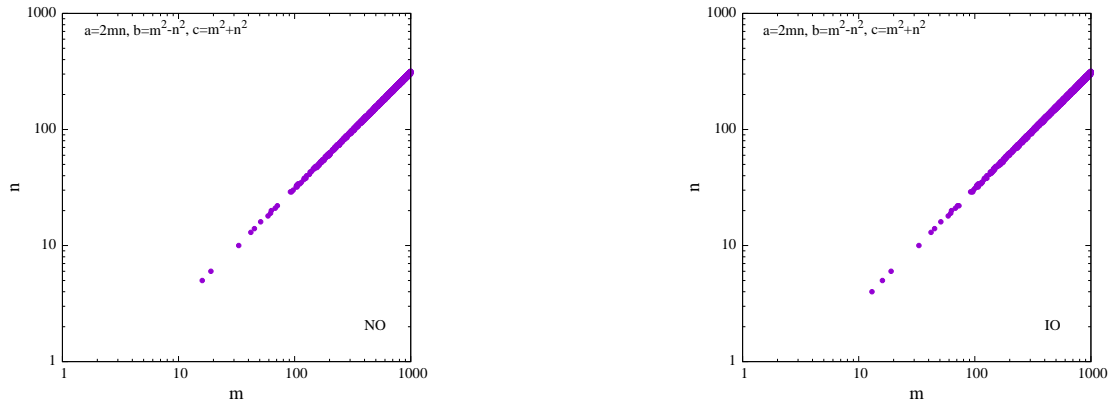


FIG. 23: Similar to Fig. 2, except for  $(a, b, c) = (2mn, m^2 - n^2, m^2 + n^2)$  and  $(U_{\text{PM}})_{C2}$ .

Fig. 25 is the same as Fig. 11, except for  $(a, b, c) = (2mn, m^2 - n^2, m^2 + n^2)$  and  $(U_{\text{PM}})_{C2}$ . The key observations from Fig. 25 are as follows:

- $\theta$  exists to satisfy the  $3\sigma$  region of  $s_{13}^2$  and  $s_{12}^2$ .
- The range of  $\theta$  satisfying the  $3\sigma$  region of  $s_{13}^2$  was limited to  $0.170 \text{ rad} \leq \theta \leq 0.190 \text{ rad}$ .
- If the range of  $\theta$  was  $0.170 \text{ rad} \leq \theta \leq 0.190 \text{ rad}$ ,  $s_{12}^2$  was within the  $3\sigma$  region of  $s_{12}^2$ . However, it exceeded the best-fit value.

Fig. 26 is the same as Fig. 5, except for  $(a, b, c) = (2mn, m^2 - n^2, m^2 + n^2)$  and  $(U_{\text{PM}})_{C2}$ . Fig. 27 is the same as Fig. 6, except for  $(a, b, c) = (2mn, m^2 - n^2, m^2 + n^2)$  and  $(U_{\text{PM}})_{C1}$ . The key observations from Fig. 26 and Fig. 27 are as follows:

- $\theta$  and  $\phi$  exist to satisfy the  $3\sigma$  region of  $s_{23}^2$ .
- This combination of  $m$  and  $n$  satisfies the best-fit value for IO.
- This combination of  $m$  and  $n$  does not satisfy the best-fit value for NO.

- If  $s_{13}^2$  aligns with the best-fit value,  $s_{23}^2$  was close to the upper limit of the  $3\sigma$  region.
- As shown in Fig. 27, the range of  $\phi$  satisfying the  $3\sigma$  region of  $s_{23}^2$  was limited to  $0 \text{ rad} \leq \phi \leq 1.0 \text{ rad}$  and  $5.3 \text{ rad} \leq \phi \leq 2\pi \text{ rad}$ .

Fig. 28 is the same as Fig. 7, except for  $(a, b, c) = (2mn, m^2 - n^2, m^2 + n^2)$  and  $(U_{\text{PM}})_{C2}$ . Fig. 29 is the same as Fig. 8, except for  $(a, b, c) = (2mn, m^2 - n^2, m^2 + n^2)$  and  $(U_{\text{PM}})_{C2}$ . The key observations from Figs. 28 and 29 are as follows:

- No difference was observed in the  $\delta$  for different combinations of  $m$  and  $n$ .
- As shown in Fig. 29, the range of  $\phi$  satisfying the  $3\sigma$  region of  $\delta$  was limited to  $2.6 \text{ rad} \leq \phi \leq 6.0 \text{ rad}$ .

## V. $Z_2$ SYMMETRY

The topic of symmetry is crucial in neutrino physics. As an example, a texture of the neutrino mass matrix based on the  $A_n$  or  $S_n$  symmetry has been proposed



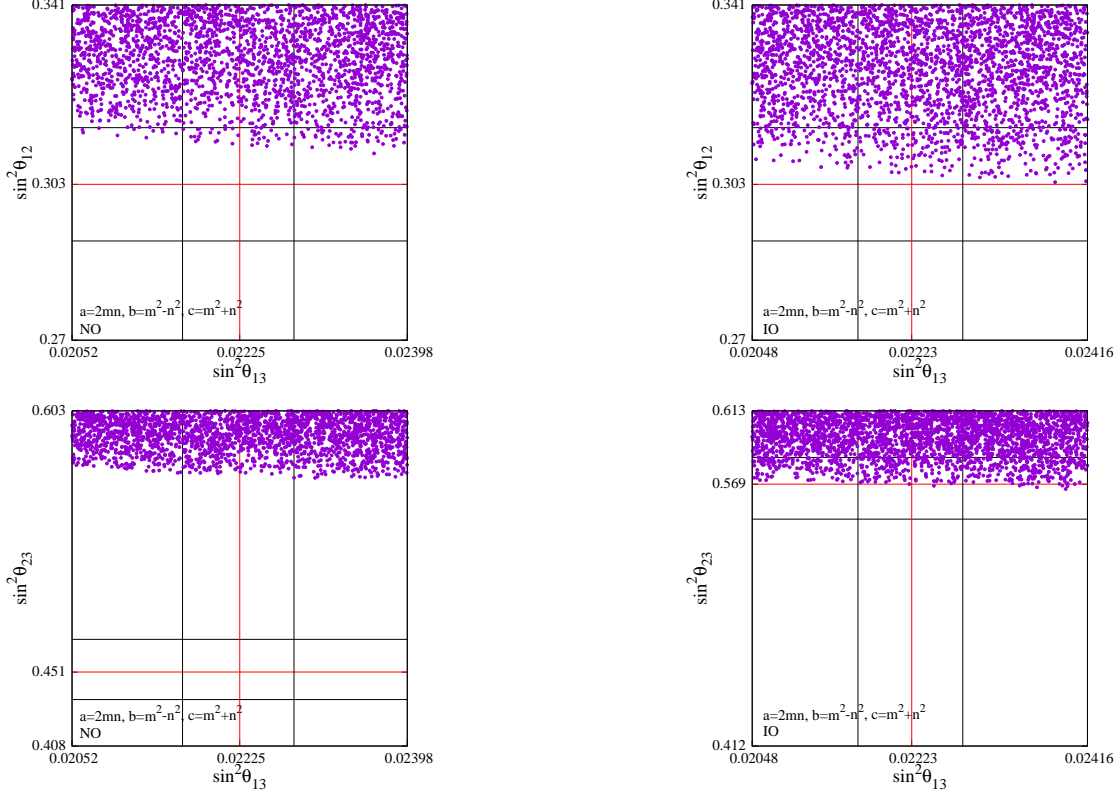


FIG. 24: Similar to Fig. 3, except for  $(a, b, c) = (2mn, m^2 - n^2, m^2 + n^2)$  and  $(U_{\text{PM}})_{C2}$ .

Ref. [19]. Discussions regarding the  $Z_2$  symmetry are conducted in the context of TBM or TM mixing models [20–22]. Ref. [23] discusses the  $Z_2$  symmetry of the mixing matrix proposed in Ref. [23]. Our PM exhibits  $Z_2$  symmetry. Herein, we discuss the  $Z_2$  symmetry of PM.

Assuming that the mass matrix of charged leptons is diagonal and real, the neutrino mass matrix,  $M_\nu$ , is as follows:

$$M_\nu = U^* \text{diag}(m_1, m_2, m_3) U^\dagger = \begin{pmatrix} A & B & C \\ B & D & E \\ C & E & F \end{pmatrix}, \quad (39)$$

where  $m_1, m_2$ , and  $m_3$  are the neutrino mass eigenvalues.

If  $M_\nu$  satisfies the transformation,

$$G^T M_\nu G = M_\nu, \quad G^2 = \text{diag}(1, 1, 1). \quad (40)$$

$M_\nu$  is invariant under  $Z_2$  symmetry[20]. In this context,  $G$  is expressed as follows:

$$G = g_1 v_1 v_1^\dagger + g_2 v_2 v_2^\dagger + g_3 v_3 v_3^\dagger, \quad (41)$$

where  $v_1, v_2$ , and  $v_3$  are column vectors of the mixing matrix, and one of the eigenvalues among  $g_1, g_2$ , and  $g_3$  was equal to  $-1$  (1). The remaining two eigenvalues were equal to 1 ( $-1$ )[20–22].

The column vectors of the PM are

$$\begin{aligned} v_1 &= \left( \frac{b}{c}, -\frac{a^2}{c^2}, \frac{ab}{c^2} \right)^T, \\ v_2 &= \left( \frac{a}{c}, -\frac{ab}{c^2}, -\frac{b^2}{c^2} \right)^T, \\ v_3 &= \left( 0, \frac{b}{c}, \frac{a}{c} \right)^T. \end{aligned} \quad (42)$$

Based on Eq. (41),  $G_i$  ( $i = 1, 2, 3$ ) can be expressed as

$$\begin{aligned} G_1 &= -v_1 (v_1)^\dagger + v_2 (v_2)^\dagger + v_3 (v_3)^\dagger \\ &= \begin{pmatrix} \frac{(a-b)(a+b)}{c^2} & \frac{2a^2b}{c^3} & -\frac{2ab^2}{c^3} \\ \frac{2a^2b}{c^3} & \frac{-a^4+a^2b^2+b^2c^2}{c^4} & \frac{ab(a^2-b^2+c^2)}{c^4} \\ -\frac{2ab^2}{c^3} & \frac{ab(a^2-b^2+c^2)}{c^4} & \frac{b^4+a^2(c-b)(c+b)}{c^4} \end{pmatrix} \end{aligned} \quad (43)$$

$$\begin{aligned} G_2 &= v_1 (v_1)^\dagger - v_2 (v_2)^\dagger + v_3 (v_3)^\dagger \\ &= \begin{pmatrix} \frac{(b+a)(b-a)}{c^2} & -\frac{2a^2b}{c^3} & \frac{2ab^2}{c^3} \\ -\frac{2a^2b}{c^3} & \frac{a^4-a^2b^2+b^2c^2}{c^4} & \frac{ab(-a^2+b^2+c^2)}{c^4} \\ \frac{2ab^2}{c^3} & \frac{ab(-a^2+b^2+c^2)}{c^4} & \frac{-b^4+a^2(b^2+c^2)}{c^4} \end{pmatrix} \end{aligned} \quad (44)$$

and,

$$G_3 = v_1 (v_1)^\dagger + v_2 (v_2)^\dagger - v_3 (v_3)^\dagger$$



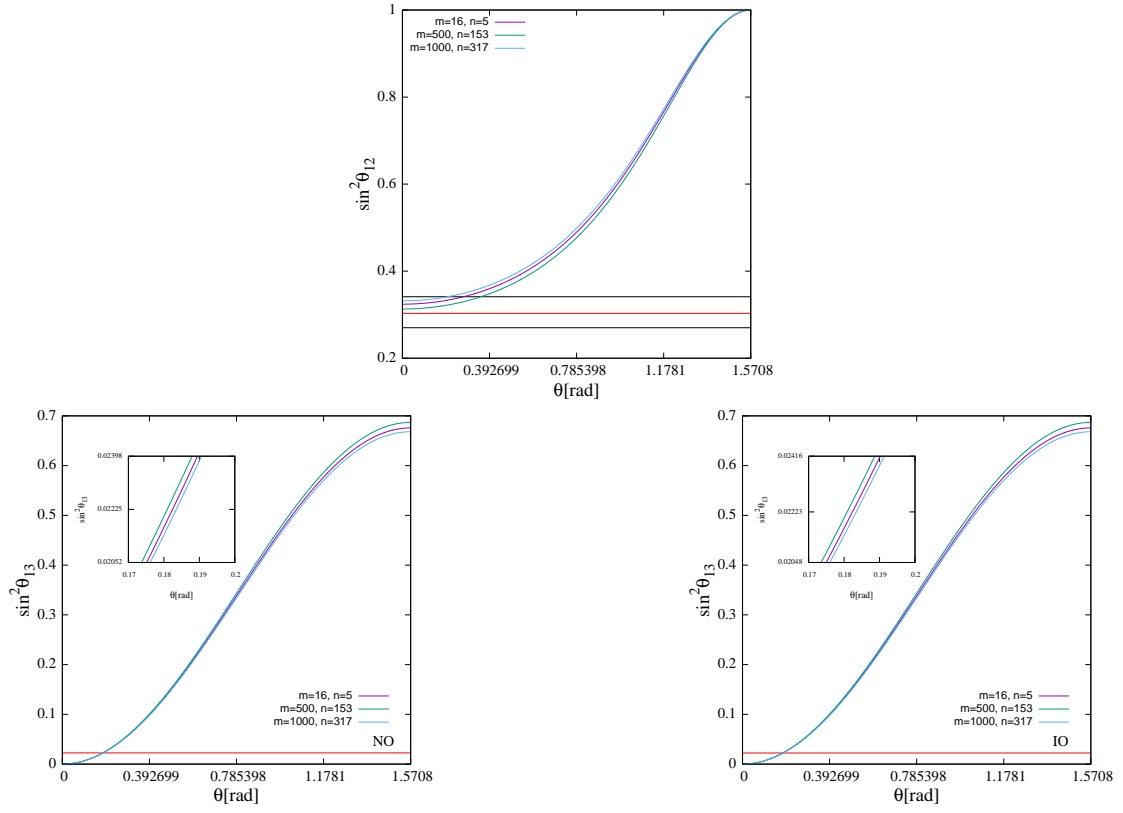


FIG. 25: Similar to Fig. 4, except for  $(a, b, c) = (2mn, m^2 - n^2, m^2 + n^2)$  and  $(U_{\text{PM}})_{C2}$ . We selected  $(m, n) = (16, 5), (500, 153), (1000, 317)$ .

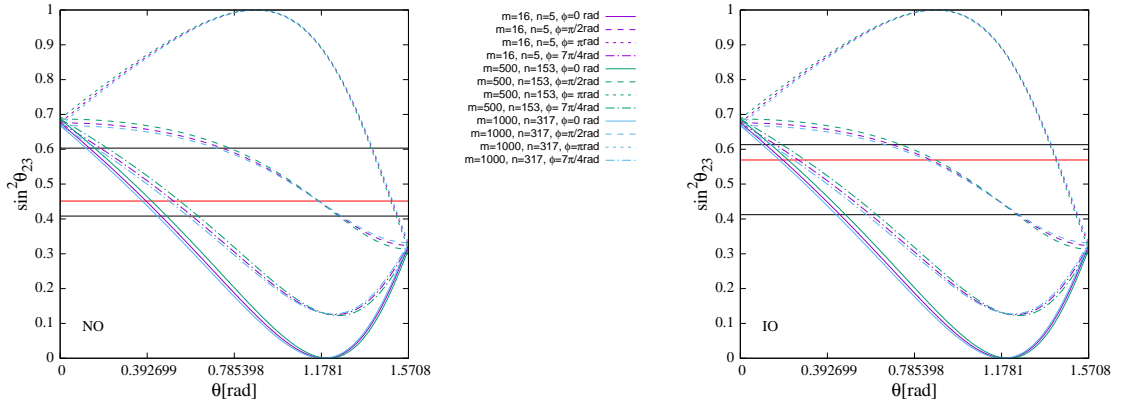


FIG. 26: Similar to Fig. 5, except for  $(a, b, c) = (2mn, m^2 - n^2, m^2 + n^2)$  and  $(U_{\text{PM}})_{C2}$ . We selected  $(m, n) = (16, 5), (500, 153), (1000, 317)$  and  $\phi = 0, \frac{\pi}{2}, \pi, \frac{7\pi}{4}$ .

$$= \begin{pmatrix} \frac{a^2+b^2}{c^2} & 0 & 0 \\ 0 & \frac{a^4+a^2b^2-b^2c^2}{c^4} & -\frac{ab(a^2+b^2+c^2)}{c^4} \\ 0 & -\frac{ab(a^2+b^2+c^2)}{c^4} & \frac{b^4+a^2(b-c)(b+c)}{c^4} \end{pmatrix}, (45)$$

where  $G_1^2 = G_2^2 = G_3^2 = \text{diag}(1, 1, 1)$ .

The neutrino mass matrix obtained from  $(U_{\text{PM}})_{C1}$  is written as follows:

$$M_{(U_{\text{PM}})_{C1}} = (U_{\text{PM}})_{C1}^* \text{diag}(m_1, m_2, m_3) (U_{\text{PM}})_{C1}^\dagger$$

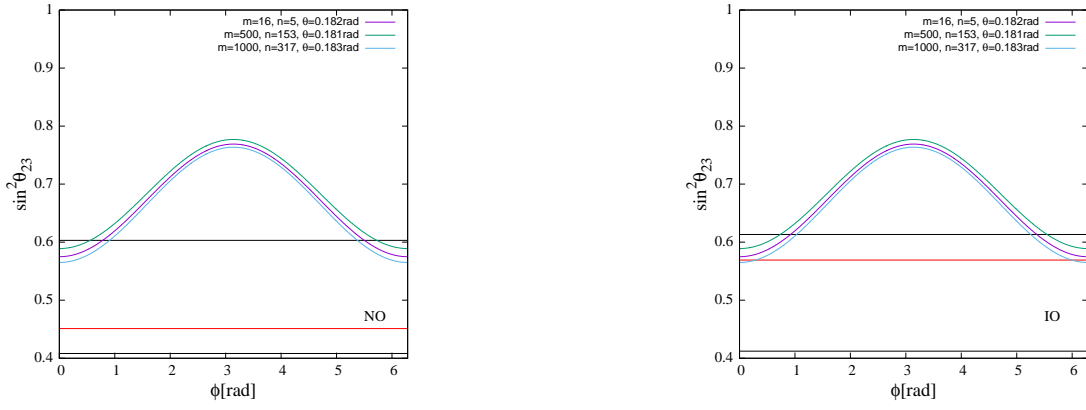


FIG. 27: Similar to Fig. 6, except for  $(a, b, c) = (2mn, m^2 - n^2, m^2 + n^2)$  and  $(U_{\text{PM}})_{C2}$ . We selected  $(m, n) = (16, 5), (500, 153), (1000, 317)$ .

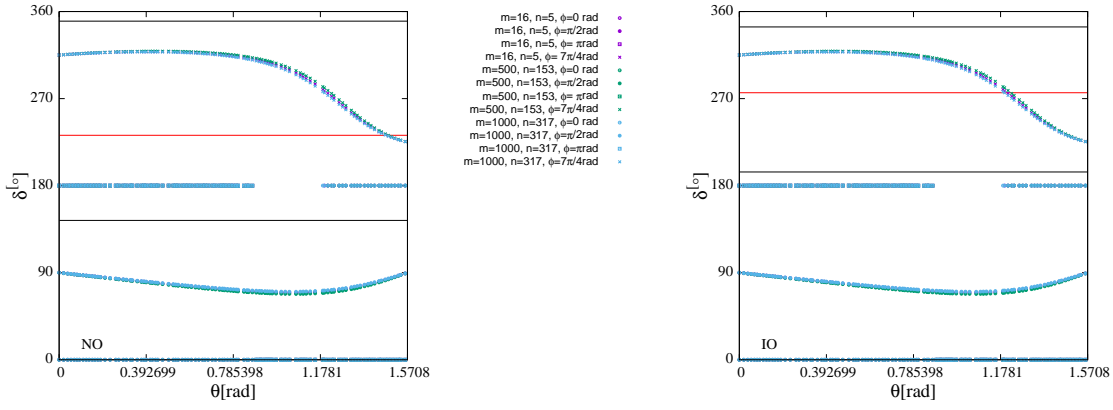


FIG. 28: Similar to Fig. 7, except for  $(a, b, c) = (2mn, m^2 - n^2, m^2 + n^2)$  and  $(U_{\text{PM}})_{C2}$ . We selected  $(m, n) = (16, 5), (500, 153), (1000, 317)$  and  $\phi = 0, \frac{\pi}{2}, \pi, \frac{7\pi}{4}$ .

$$= \begin{pmatrix} A & B & C \\ B & D & \frac{a^4 B - b^4 B - a^3 b C - a^2 b \{bB + c(A-D)\}}{ab^2 c} \\ C & \frac{a^4 B - b^4 B - a^3 b C - a^2 b \{bB + c(A-D)\}}{ab^2 c} & \frac{a^5 B + ab^3(cA - bB) - a^4 b C - b^5 C - a^3 b \{2bB + c(A-D)\}}{ab^3 c} \end{pmatrix}. \quad (46)$$

The neutrino mass matrix obtained from  $(U_{\text{PM}})_{C2}$  is written as follows:

$$M_{(U_{\text{PM}})_{C2}} = (U_{\text{PM}})_{C2}^* \text{diag}(m_1, m_2, m_3) (U_{\text{PM}})_{C2}^\dagger$$

$$= \begin{pmatrix} A & B & C \\ B & D & \frac{a^3 B + b^3 C + abc(D-A)}{b^2 c} \\ C & \frac{a^3 B + b^3 C + abc(D-A)}{b^2 c} & \frac{a^5 B + ab^3(cA + bB) + a^4 b C + 2a^2 b^3 C - b^5 C + a^3 bc(D-A)}{ab^3 c} \end{pmatrix}. \quad (47)$$

Considering that these neutrino mass matrices,  $M_{(U_{\text{PM}})_{C1}}$  and  $M_{(U_{\text{PM}})_{C2}}$ , were satisfied through transformation

$$G_1^T M_{(U_{\text{PM}})_{C1}} G_1 = M_{(U_{\text{PM}})_{C1}}, \quad (48)$$

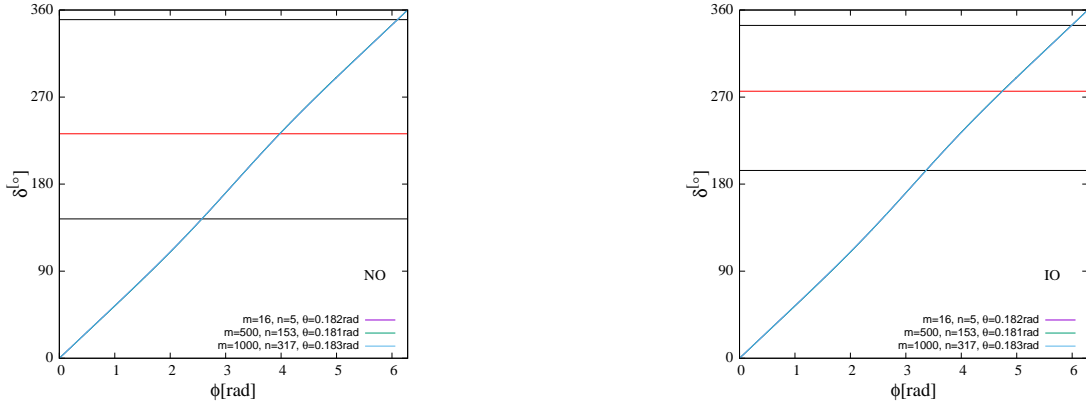


FIG. 29: Similar to Fig. 8, except for  $(a, b, c) = (2mn, m^2 - n^2, m^2 + n^2)$  and  $(U_{\text{PM}})_{C_2}$ . We selected  $(m, n) = (16, 5), (500, 153), (1000, 317)$ .

and

$$G_2^T M_{(U_{\text{PM}})_{C_2}} G_2 = M_{(U_{\text{PM}})_{C_2}}, \quad (49)$$

they were invariant under  $Z_2$  symmetry.

## VI. SUMMARY

Here, we focused on primitive Pythagorean triples [1–9] to construct a neutrino mixing model. Primitive Pythagorean triples refer to sets of three natural numbers  $(a, b, c)$  satisfying  $c^2 = a^2 + b^2$ . For instance, in the triangle,  $(3, 4, 5)$ , the three internal angles are  $(36.87^\circ, 53.13^\circ, 90.00^\circ)$ . Among these,  $(36.87^\circ, 53.13^\circ)$  closely approximate the upper limit of  $3\sigma$  for the solar neutrino mixing angle,  $35.74^\circ$ , and the upper limit of the  $3\sigma$  atmospheric mixing angle,  $51.0^\circ$  ( $51.5^\circ$ ), in the case of NO (IO).

First, the relationship between primitive Pythagorean triples and neutrino mixing angles,  $\theta_{12}$  and  $\theta_{23}$ , is as follows:

$$s_{12} = \frac{a}{c}, \quad s_{23} = \frac{b}{c}, \quad (50)$$

where the relationship among  $a$ ,  $b$ , and  $c$  is described by  $a < b < c$ . From this relationship, we constructed the neutrino mixing matrix  $U_{\text{PM}}$ . However, the mixing matrix predicts the vanishing reactor mixing angle. To improve the reproducibility of the reactor mixing angle, we modified  $(U_{\text{PM}})_{C_1} = U_{\text{PM}} U_{23}$  ( $(U_{\text{PM}})_{C_2} = U_{\text{PM}} U_{13}$ )

where  $U_{23}$  and  $U_{13}$  are

$$U_{23} = \begin{pmatrix} 1 & 0 & 0 \\ 0 & \cos \theta & \sin \theta e^{-i\phi} \\ 0 & -\sin \theta e^{i\phi} & \cos \theta \end{pmatrix} \quad (51)$$

and

$$U_{13} = \begin{pmatrix} \cos \theta & 0 & \sin \theta e^{-i\phi} \\ 0 & 1 & 0 \\ -\sin \theta e^{i\phi} & 0 & \cos \theta \end{pmatrix}. \quad (52)$$

Consequently, we obtained a new neutrino mixing model related to primitive Pythagorean triples that satisfies the observed values.

We showed that the neutrino mass matrix,  $M_{(U_{\text{PM}})_{C_1}}$  ( $M_{(U_{\text{PM}})_{C_2}}$ ), obtained from  $(U_{\text{PM}})_{C_1}$  ( $(U_{\text{PM}})_{C_2}$ ) was invariant under  $Z_2$  symmetry.

Finally, in this paper, we modified  $U_{\text{PM}}$  into  $U_{\text{PM}} U_{23}$  ( $U_{\text{PM}} U_{13}$ ). We would like to consider the charged lepton mixing,  $U_e$ , as in Ref. [24] and the texture of the neutrino mass matrix in the future. In the present numerical calculation results, the simplest primitive Pythagorean triple,  $(3, 4, 5)$ , did not match the observed values. The simplest primitive Pythagorean triple  $(3, 4, 5)$  shared relations with other primitive Pythagorean triples, as observed in Ref. [6–9]. Such relationships are referred to as the trees of primitive Pythagorean triples. We would like to investigate the relationship between the trees of primitive Pythagorean triples and the neutrino mixing in the future.

- 
- [1] K. R. Williams, TRIPLES: Applications of Pythagorean Triples (Inspiration Books, 2017)
  - [2] G. J. Martens, arXiv:2112.09553 [math.GM].
  - [3] J. Kocik, Advances in Applied Clifford Algebras. **17**, 71–93 (2007).

- [4] A. Schmelzer, and S. Chetty, arXiv:2102.03451 [math.NT].
- [5] A. Yekutieli, arXiv:2101.12166 [math.NT].
- [6] B. Cha, E. Nguuyen, and B. Tauber, J. of Number Theor. **185**, 218–256 (2018).

- [7] P. Deriy, arXiv:2310.15174 [math.HO].
- [8] H. Lee. Price, arXiv:0809.4324 [math.HO].
- [9] R. C. Alperin, arXiv:0010281 [math.HO].
- [10] B. Pontecorvo, Sov. Phys. JETP. **6**, 429 (1957).
- [11] B. Pontecorvo, Sov. Phys. JETP. **7**, 172 (1958).
- [12] Z. Maki, M. Nakagawa and S. Sakata, Prog. Theor. Phys. **28**, 870 (1962).
- [13] M. Tanabashi *et al.* (Particle Data Group), Phys. Rev. D **98**, 030001 (2018).
- [14] C. Jarlskog, Phys. Rev. Lett. **55**, 1039 (1985).
- [15] I. Esteban, M. C. Gonzalez-Garcia, M. Maltoni, T. Schwetz, and A. Zhou, J. High Energy Phys. **09**, 178 (2020). See also, NuFIT 5.2 (2022), [www.nu-fit.org](http://www.nu-fit.org).
- [16] Z. Z. Xing and S. Zhou, Phys. Lett. B **653**, 278 (2007).
- [17] J. D. Bjorken, P. F. Harrison, and W. G. Scott, Phys. Rev. D **74**, 073012 (2006).
- [18] K. Pearson, Proc. R. Soc. Lond. **58**, 240 (1895).
- [19] G. Altarelli and F. Feruglio, Rev. Mod. Phys. **82**, 2701 (2010).
- [20] C. S. Lam, Phys. Rev. D **74**, 113004 (2006).
- [21] C. S. Lam, Phys. Lett. B **656**, 193 (2007).
- [22] C. S. Lam, Phys. Rev. Lett. **101**, 121602 (2008).
- [23] D. A. Dicus, S. -F. Ge, and W. W. Repko, Phys. Rev. D **83**, 093007 (2011).
- [24] S. T. Petcov, Nucl. Phys. B **892**, 400-428 (2015).